

Categorization of 31 computational methods to detect spatially variable genes from spatially resolved transcriptomics data

Guanao Yan^{1,†}, Shuo Harper Hua^{2,†}, and Jingyi Jessica Li^{1,3,4,5,6,*}

Abstract

In the analysis of spatially resolved transcriptomics data, detecting spatially variable genes (SVGs) is crucial. Numerous computational methods exist, but varying SVG definitions and methodologies lead to incomparable results. We review 31 state-of-the-art methods, categorizing SVGs into three types: overall, cell-type-specific, and spatial-domain-marker SVGs. Our review explains the intuitions underlying these methods, summarizes their applications, and categorizes the hypothesis tests they use in the trade-off between generality and specificity for SVG detection. We discuss challenges in SVG detection and propose future directions for improvement. Our review offers insights for method developers and users, advocating for category-specific benchmarking.

¹ Department of Statistics, University of California, Los Angeles, CA 90095-1554

² Department of Biomedical Data Science, Stanford University, Stanford, CA 94305

³ Department of Human Genetics, University of California, Los Angeles, CA 90095-7088

⁴ Department of Computational Medicine, University of California, Los Angeles, CA 90095-1766

⁵ Department of Biostatistics, University of California, Los Angeles, CA 90095-1772

⁶ Radcliffe Institute for Advanced Study, Harvard University, Cambridge, MA 02138

[†] These authors contributed equally

* To whom correspondence should be addressed. Email: jli@stat.ucla.edu

1 Introduction

In multicellular organisms, cells work cooperatively in tissues and organs to fulfill biological functions. Measuring cells' spatial locations along with transcriptome profiles can help unravel collaborative cell organizations and molecular mechanisms in tissues and organs [1]. Spatially resolved transcriptomics (SRT) technologies have been rapidly evolving to enable high-throughput profiling of transcriptomes at spatial locations, which may represent single cells or groups of cells, in a tissue slice. SRT data provide unprecedented insights into genes' spatial expression patterns, tissue's cellular organizations, and cell-cell communications [2].

To date, major SRT technologies are either imaging-based or sequencing-based, and the two types of technologies have complementary advantages [1]. Imaging-based SRT technologies use fluorescence in situ hybridization (FISH) to measure the expression levels of selected target genes at the single-cell or subcellular spatial resolution [1]. Examples of imaging-based SRT technologies include in situ sequencing (ISS) [3], sequential fluorescence in situ hybridization (seqFISH) [4–6], multiplexed error-robust fluorescence in situ hybridization (MERFISH) [7], STARmap [8], ExSeq [9], and 10x Xenium [10]. In parallel, sequencing-based SRT technologies include Spatial Transcriptomics [5], 10x Visium [11], Slide-seq [12], and GeoMx [13], all of which capture transcriptome-wide gene expression at a lower spatial resolution, with each spot's diameter between $10\ \mu\text{m}$ and $100\ \mu\text{m}$, so each spot contains multiple cells of possibly different types [1]. Note that recently developed sequencing-based SRT [14, 15] can achieve a higher, even single-cell, spatial resolution, with the spot diameter reduced to below $1\ \mu\text{m}$, despite the significantly higher cost.

Although imaging-based and sequencing-based SRT technologies have different spatial resolutions, for simplicity, we use the same term “spots” to refer to the measured spatial locations for both technologies in this review. Hence, SRT data encompass two components: (1) an expression count matrix of p genes at n spots and (2) a spatial coordinate matrix containing the two-dimensional (2D) coordinates of n spots.

As with other types of high-throughput data where hundreds or thousands of genes are measured simultaneously, a crucial early step of SRT data analysis is the identification of informative genes. Prior to SRT data, single-cell RNA-seq data contain gene expression profiles of single cells without spatial information. In typical single-cell RNA-seq data analysis (Fig. 1), highly variable gene (HVG) detection methods are used to screen a proportion of genes (e.g., 10%–20%) with the largest variances (adjusting for cell library sizes in several methods) to reduce the dataset's dimensionality (from p genes to a smaller number of HVGs) and remove the unimportant variations of many genes. The underlying assumption of HVG detection is that genes exhibiting significant expression variations across single cells are more likely to reflect biological variations rather than technical variations caused by sampling effects in sequencing. Analogous to single-cell RNA-seq data analysis, SRT data analysis typically includes an early step to detect *spatially variable genes* (SVGs), which conceptually generalize HVGs by including the spatial information (Fig. 1).

Intuitively, SVGs are genes whose gene expression levels exhibit non-random, informative spatial patterns.

In single-cell RNA-seq data analysis (Fig. 1), common steps after HVG detection include cell clustering and differentially expressed gene (DEG) detection. The goal of cell clustering is to identify potential cell types, and subsequent DEG detection aims to find genes that are more highly expressed in specific clusters. The resulting DEGs are then used to annotate the cell clusters as particular cell types, serving as cell-type markers. Similarly, in SRT data analysis, following SVG detection, spots are often partitioned into spatial domains, where each domain contains proximal spots exhibiting similar gene expression profiles. Parallel to DEG detection between clusters in single-cell RNA-seq data analysis, DEGs can be identified between spatial domains and serve as spatial-domain markers.

Many computational methods have been developed to detect SVGs. However, the SVG definitions in these methods lack consensus, resulting in diverse meanings for the detected SVGs and making understanding difficult. Consequently, the inconsistent definitions of SVGs may lead to ambiguous usage of computational methods. Although 19 methods were reviewed previously [16], the review did not categorize SVG definitions but only focused on summarizing the methodologies, including the input data type (count data vs. normalized data), algorithm type (model-based vs. model-free), statistical paradigm (frequentist vs. Bayesian), the availability of false discovery rate (FDR) control, etc. Nor did the review discuss the biological implications and downstream applications of SVGs.

Motivated by this gap in understanding SVGs, here we review 31 peer-reviewed SVG detection methods (Figs. 2–3) and define three SVG categories: *overall SVGs*, *cell-type-specific SVGs*, and *spatial-domain-marker SVGs*. For the first time, our review unveils the biological significance underpinning the three categories of SVGs, summarizes the frequentist hypothesis tests implemented in 21 SVG detection methods, and discusses the limitations of existing methods and outlines future directions for improvement. Moreover, we construct a hierarchy to summarize the 31 SVG detection methods in terms of methodological differences (Fig. 4 and list the technical details in Tables 1–3).

Methods for detecting the three SVG categories serve different purposes (Fig. 2). The detection of overall SVGs screens informative genes for downstream analysis, such as spatial domain identification. Detecting cell-type-specific SVGs aims to reveal spatial variation within a cell type and help identify distinct cell subpopulations or states within cell types. Finally, spatial-domain-marker SVG detection is used to find marker genes to annotate and interpret spatial domains already detected. These markers help understand the molecular mechanisms underlying spatial domains and assist in annotating tissue layers in other datasets.

The relationship among the three SVG categories depends on the detection methods, particularly the null and alternative hypotheses they employ. For example, if an overall SVG detection method uses the null hypothesis that a non-SVG's expression is independent of spatial location and the alternative hypothesis that all other genes are SVGs, then its SVGs should theoretically

include any cell-type-specific SVGs and spatial-domain-marker SVGs. However, if the method’s alternative hypothesis is defined for a specific spatial expression pattern, its SVGs may not encompass some cell-type-specific SVGs or spatial-domain-marker SVGs. We provide a comprehensive discussion on the frequentist hypothesis tests implemented by 21 SVG detection methods in the Section “Theoretical characterization of SVG detection methods that use frequentist hypothesis tests.”

Although three benchmark studies were conducted to compare SVG detection methods [17–19], they have three major differences from our review. First, the benchmark studies performed numerical comparisons of SVG detection methods, while our review focuses on categorizing methods conceptually and methodologically. Second, the benchmark studies did not categorize SVGs but focused on detecting the overall SVGs by our definition. For example, spaGCN, a method that detects spatial-domain-marker SVGs, does not perform well in the benchmark study [17], possibly because the study focused on detecting overall SVGs. This observation underscores the need to categorize SVGs. Third, our review has a more comprehensive coverage of SVG detection methods: 31 peer-reviewed methods (all methods to our knowledge) compared to 14 methods (12 peer-reviewed) in [17], 7 methods in [18], and 6 methods in [19]. In summary, existing benchmark studies complement our review by providing numerical evidence to rank methods in detecting certain types of overall SVGs. Future benchmark studies are needed to compare methods within the three SVG categories and examine more types of null and alternative hypotheses.

2 Mathematical notations

To facilitate our discussion, we introduce the following mathematical notations. For each gene with expression levels (in counts or normalized) measured at n spatial spots, we use $y_i \in \mathbb{R}$ represent its expression level at spot $i = 1, \dots, n$. When gene expression levels are considered random variables, we use Y_i to emphasize the random nature.

For each spot $i = 1, \dots, n$, we denote its 2D spatial location as $\mathbf{s}_i = (s_{i1}, s_{i2})^\top \in \mathbb{R}^2$. The spatial coordinates of all n spots are represented by the matrix $\mathbf{s} = [\mathbf{s}_1, \dots, \mathbf{s}_n]^\top \in \mathbb{R}^{n \times 2}$, where each row corresponds to a spot. When spots are annotated with L spatial domain labels, the spatial-domain indicator vector for spot i is $\mathbf{d}_i = (d_{i1}, \dots, d_{iL})^\top \in \{0, 1\}^L$, with $\sum_{l=1}^L d_{il} = 1$; that is, $d_{il} = 1$ means that spot i belongs to spatial domain l . When spots are annotated with K cell type labels, the cell-type proportion vector for spot i is $\mathbf{c}_i = (c_{i1}, \dots, c_{iK})^\top \in [0, 1]^K$, where c_{ik} indicates the proportion of cell type k at spot i , with $\sum_{k=1}^K c_{ik} = 1$. In summary, each spot i has three covariate vectors: spatial location \mathbf{s}_i , spatial-domain indicator \mathbf{d}_i , and cell-type proportions \mathbf{c}_i .

3 Methods for detecting overall SVGs

We define *overall SVGs* as the most general category of SVGs detected using only SRT data without incorporating external information such as spatial domains or cell types (Fig. 2). Methods for detecting overall SVGs are generally classified into Euclidean-space-based and graph-based methods (Fig. 4). Euclidean-space-based methods analyze spots in a tissue slice by considering their locations in a 2D Euclidean space. In contrast, graph-based methods first construct a graph of spatial spots and then analyze this graph, focusing on the connections between spots rather than their Euclidean distances. Both approaches, regardless of the spatial representation they use (Euclidean space or graph), study how a gene's expression levels vary across spatial spots, examining the relationship between each gene and its spatial context.

3.1 Euclidean-space-based methods

Euclidean-space-based methods are further divided based on whether they use a kernel function to target a specific spatial pattern. Kernel-based methods utilize a kernel function to specify the covariances of spatial spots, enhancing their power to detect the targeted spatial patterns. In contrast, kernel-free methods do not use a kernel function and instead rely on other approaches to capture spatial patterns.

3.1.1 Kernel-based methods

Kernel-based methods use a pre-defined kernel function $K(\mathbf{s}_i, \mathbf{s}_j)$ to specify the covariance between spots i and j based on their spatial locations. This kernel function usually decays as the Euclidean distance between spots i and j increases. Define $\mathbf{K}(\mathbf{s}) = [K(\mathbf{s}_i, \mathbf{s}_j)]$ as the $n \times n$ matrix representing these covariances. The most commonly used kernel functions include the Gaussian kernel for detecting clustered or focal expression patterns, expressed as

$$K_G(\mathbf{s}_i, \mathbf{s}_j) = \exp\left(-\frac{\|\mathbf{s}_i - \mathbf{s}_j\|^2}{2\sigma^2}\right),$$

and the cosine kernel for detecting periodic expression patterns, denoted by

$$K_C(\mathbf{s}_i, \mathbf{s}_j) = \cos\left(2\pi \frac{\|\mathbf{s}_i - \mathbf{s}_j\|}{\phi}\right).$$

For a given gene, the variance of its expression \mathbf{Y} (subject to transformation of \mathbf{Y}) across the n spots can be decomposed into multiple variance components, one of which depends on $\mathbf{K}(\mathbf{s})$. If the contribution of this term is significantly positive according to a hypothesis test, the gene is detected as an overall SVG.

Following this general idea, nine kernel-based methods (Fig. 4) make different assumptions about the distribution of \mathbf{Y} and the variance decomposition. Below, we briefly summarize these

methods and highlight their similarities and differences.

SpatialDE [20] assumes that a gene’s normalized expression $\mathbf{Y} \in \mathbb{R}^n$ follows an n -dimensional Gaussian distribution, with a covariance matrix that includes a spatial variance component involving $\mathbf{K}(\mathbf{s})$:

$$\mathbf{Y} \sim \text{MVN}(\boldsymbol{\mu}, \sigma_s^2 \cdot \mathbf{K}(\mathbf{s}) + \delta \cdot \mathbf{I}),$$

where MVN represents a multivariate Gaussian distribution with a mean vector $\boldsymbol{\mu} \in \mathbb{R}^n$ and a covariance matrix $\sigma_s^2 \cdot \mathbf{K}(\mathbf{s}) + \delta \cdot \mathbf{I}$. Here, \mathbf{I} is an n -dimensional identity matrix, and σ_s^2 and δ are parameters representing the spatial variance component and the error variance component, respectively. This model is a realization of a Gaussian process with the kernel function $K(\cdot, \cdot)$. To determine if a gene is an overall SVG, SpatialDE employs a likelihood ratio test with the null hypothesis $H_0 : \sigma_s^2 = 0$, comparing this model with a null model that does not include the spatial variance component: $\mathbf{Y} \sim \text{MVN}(\boldsymbol{\mu}, \sigma^2 \cdot \mathbf{I})$.

Using the same model as SpatialDE, **nnSVG** [21] improves computational efficiency by replacing the Gaussian process with the nearest-neighbor Gaussian process [22], providing a scalable approximation. This enhancement allows nnSVG’s computational complexity and runtime to scale linearly with the number of spatial spots.

SOMDE [23] also follows the statistical model of SpatialDE but adds a data preprocessing step for scalability. Specifically, SOMDE condenses the original spatial spots into fewer gridding points and assigns each condensed point a "meta-expression," which aggregates a gene’s expression levels at the spots condensed into that point. After this preprocessing step, SOMDE uses the same approach as SpatialDE to detect whether the gene is an overall SVG, but it does so using the condensed points instead of the original spots.

Compared to the first three methods, **SVCA** [24] modifies the variance decomposition by adding two additional variance components:

$$\mathbf{Y} \sim \text{MVN}(\boldsymbol{\mu}, \mathbf{K}_{\text{int}} + \mathbf{K}_{\text{c-c}} + \mathbf{K}(\mathbf{s}) + \sigma^2 \cdot \mathbf{I}),$$

where \mathbf{K}_{int} denotes the intrinsic cell-state covariance, and $\mathbf{K}_{\text{c-c}}$ represents the cell-cell interaction covariance. Specifically, \mathbf{K}_{int} is defined solely using gene expression data without spatial information, while $\mathbf{K}_{\text{c-c}}$ incorporates both gene expression data and Euclidean distances among spots.

Instead of using normalized gene expression data, **SPARK** [25], **GPcounts** [26], and **BOOST-GP** [27] directly model a gene’s expression count at spot i , $Y_i \in \mathbb{N}$, using Poisson, negative binomial (NB), and zero-inflated negative binomial (ZINB) distributions, respectively. For instance, SPARK assumes that

$$Y_i \stackrel{\text{ind}}{\sim} \text{Poisson}(\mu_i(\mathbf{s}_i)), \quad i = 1, 2, \dots, n.$$

For spot i , the Poisson mean parameter $\mu_i(\mathbf{s}_i)$ is a function of the spatial location \mathbf{s}_i , specified by

$$\log(\mu_i(\mathbf{s}_i)) = \mathbf{x}_i(\mathbf{s}_i)^\top \boldsymbol{\beta} + b_i(\mathbf{s}_i) + \epsilon_i,$$

where $\mathbf{x}_i(\mathbf{s}_i)$ indicates spot i 's covariates, and $b_i(\mathbf{s}_i)$ is the random intercept at spot i . The n random intercepts, $b_1(\mathbf{s}_1), \dots, b_n(\mathbf{s}_n)$, are assumed to follow a Gaussian process with the kernel function $K(\cdot, \cdot)$:

$$(b_1(\mathbf{s}_1), b_2(\mathbf{s}_2), \dots, b_n(\mathbf{s}_n))^\top \sim \text{MVN}(0, \sigma_s^2 \cdot \mathbf{K}(\mathbf{s})).$$

To decide whether the gene is an overall SVG, SPARK tests the null hypothesis $H_0 : \sigma_s^2 = 0$. Thus, SPARK shares the same variance component test idea with SpatialDE but uses a hierarchical model, incorporating a Gaussian process in the top layer and Poisson distributions in the bottom layer, to account for count data.

Unlike the previous seven methods that use parametric models, **SPARK-X** [28] employs a non-parametric test to determine whether a gene's expression is independent of its spatial location. SPARK-X compares two $n \times n$ spot similarity matrices: one based on the gene's expression levels at the n spots and the other based on the kernel-transformed spatial locations of the n spots. To detect diverse spatial patterns, SPARK-X transforms the spatial locations $\mathbf{s}_i = (s_{i1}, s_{i2})$, $i = 1, \dots, n$, using two kernel-based functions: a Gaussian transformation $s'_{il} = \exp\left(\frac{-s_{il}^2}{2\sigma_l^2}\right)$, $l = 1, 2$, to detect clustered or focal patterns, and a cosine transformation $s'_{il} = \cos\left(\frac{2\pi s_{il}}{\phi_l}\right)$, $l = 1, 2$, to detect periodic patterns, where $\sigma_1, \sigma_2, \phi_1$, and ϕ_2 are tuning parameters.

singlecellHaystack [29] is a test of independence between a gene's expression level and its spatial location. It involves two pre-processing steps: first, the gene's expression levels at various spots are binarized into two states: detected and undetected; second, the 2D Euclidean space of a tissue slice is divided into a grid along both axes, with intersection points defined as grid points, serving as coarse spatial coordinates. After pre-processing, the method tests if the gene's two expression states are randomly distributed across the grid points. If they are not, the gene is considered an SVG. **singlecellHaystack** uses a 2D independent Gaussian kernel, assuming independence of the two dimensions of the Euclidean space, to define three distributions of grid points: a reference distribution based on all spatial spots, a conditional distribution based on spatial spots in the detected state, and another conditional distribution based on spatial spots in the undetected state. The test statistic is defined as the sum of two Kullback-Leibler (KL) divergences, each representing the deviance of one conditional distribution from the reference distribution. Intuitively, the larger the test statistic, the more likely the gene is an overall SVG. Finally, the test statistic is converted to a p-value using a permutation test, which shuffles the gene's expression levels across spots.

To summarize, all nine kernel-based methods require pre-specification of the kernel function $K(\cdot, \cdot)$ to target specific spatial patterns. Consequently, the statistical power of these methods depends on how well the kernel function captures the spatial expression patterns of biologically informative genes in the SRT data. Due to the limited choices and subjectivity of kernel functions, these methods may be insufficient for detecting complex spatial expression patterns, such as those found in cancer SRT data.

3.1.2 Kernel-free methods

Eight kernel-free methods employ diverse approaches to detect overall SVGs without relying on pre-specified kernel functions (Fig. 4). Instead, they utilize various statistical and computational techniques to capture spatial patterns. Below, we briefly summarize each method.

Trendsceek [30] tests if a gene’s expression level is dependent of the spatial location using a marked point process, which models the joint probability distribution of spatial locations s_i , $i = 1, \dots, n$, as “points” and a given gene’s expression levels y_i , $i = 1, \dots, n$, as “marks.” If deemed dependent, the gene is detected as an overall SVG. For a pair of points (s_i, s_j) and their corresponding marks (y_i, y_j) , Trendsceek parameterizes their joint probability density by the distance (called “radius”) $r_{ij} = |s_i - s_j|$ and the marks y_i, y_j as $f(y_i, y_j, r_{ij})$. Formally, the dependence of the gene’s expression on spatial location is formulated as a conditional density function given the radius $r_{ij} = r$:

$$g(r) = M(y_i, y_j | r_{ij} = r) = \frac{f(y_1, y_2, r)}{f(r)}.$$

The univariate function $g(\cdot)$ can then be summarized into four mark-segregation summary statistics as functions of the radius r , such as Stoyan’s mark-correlation function. To test if the gene is an overall SVG, Trendsceek implements a permutation test by sampling marks without replacement and randomly reassigning them to points. For each radius r , summary statistics are calculated and compared to the null distributions derived from the permutations to obtain p-values, which are then combined into a single p-value across all radius values.

MULTILAYER [31], similar to singlecellHaystack, discretizes spatial spots for each gene based on the gene’s expression levels. The discretization procedure in MULTILAYER consists of three steps. First, each spot receives a \log_2 fold change, defined as the ratio of the gene’s normalized expression level at the spot to its average normalized expression level across all spots. The \log_2 fold changes with absolute values greater than 1 are truncated to 1 with the corresponding sign. Second, MULTILAYER applies agglomerative clustering to the spots based on the \log_2 fold change values, using a pre-specified distance threshold. Third, if a cluster contains contiguous spots with all positive \log_2 fold change values, MULTILAYER assigns the cluster a label of “1.” Finally, MULTILAYER uses the size of the largest cluster labeled as “1” as a summary statistic for the gene and ranks genes from high to low based on this statistic. Thus, if a gene has a large contiguous cluster labeled as “1,” it is considered to have a high-expression neighborhood and is regarded as an overall SVG. However, MULTILAYER does not provide statistical significance for its overall SVG ranking.

sepal [32] is a diffusion-process-based method [3] that identifies a gene as an overall SVG if its spatial expression pattern deviates from randomness. To quantify this deviation, sepal simulates a diffusion process from the gene’s observed expression pattern until it converges to randomness, using the convergence time as a measure. The longer the convergence time, the more likely the gene is an overall SVG. However, this method ranks genes but does not provide statistical

significance for the detected overall SVGs. Specifically, *sepal* uses the diffusion equation based on Fick's second law [33] to simulate the diffusion of the gene's transcripts in the 2D Euclidean space of a tissue slice.

BSP [34] is built upon the intuition that an overall SVG should have its spatial expression pattern vary significantly at different spatial resolutions; otherwise, the pattern should remain consistent. To implement this, BSP follows a four-step procedure. First, for each spot, it defines "big" and "small" patches consisting of neighboring spots within pre-specified large and small radii, respectively, so each spot has one big patch and one small patch. Second, for each gene, BSP calculates the average expression levels within the big patches and the variance of these averages, then similarly calculates the variance for the small patches. Third, BSP uses the ratio of the big-patch variance to the small-patch variance as a statistic to summarize the change in the gene's expression pattern with changing spatial resolution. Finally, BSP ranks genes by this statistic, identifying those with large values as overall SVGs. Although BSP attempts frequentist inference by defining a null distribution for its statistic, this null distribution is improperly defined as a distribution fitted to the statistic values of all genes, implying that all genes are non-SVGs. Therefore, we do not consider BSP to provide valid statistical inference in our review.

PROST [35] determines if a given gene is an overall SVG based on computer image segmentation. First, treating the gene's spatial expression in a tissue slice as an image, PROST applies image segmentation techniques to detect multiple foreground regions, where the gene is considered expressed, and one background region, where the gene is treated as unexpressed. Second, PROST defines two statistics: (1) a significance factor summarizing the overall elevation of the gene's expression from the background region to the foreground regions, and (2) a separability factor measuring the overall homogeneity of the gene's expression within each foreground region. Finally, PROST combines these two statistics into a single index. Based on this index, PROST ranks genes from high to low and selects the top-ranking genes as overall SVGs. Although PROST performs frequentist statistical tests, they are for Moran's I [36] rather than its index. Therefore, we do not consider PROST to provide valid statistical inference in our review.

SPADE [37] leverages the hematoxylin-and-eosin (H&E) image accompanying the SRT data (e.g., 10x Visium) to detect overall SVGs. It defines a gene as an overall SVG if the gene's expression levels can be predicted by H&E features, which are extracted by a pre-trained convolutional neural network and expected to contain critical spatial information, in a linear model. Specifically, SPADE first performs principal component analysis (PCA) on the 512 H&E features for dimensionality reduction. Then, it tests if the resulting principal components can predict the gene's expression levels in a linear model. If so, the gene is defined as an overall SVG.

BOOST-MI [38] and **BOOST-HMI** [39] are Bayesian methods that detect overall SVGs based on the Ising model and its extension to the geostatistical mark interaction model, respectively. The Ising model, historically used to model ferromagnetism, represents each magnetic moment (or spin) in a material as a discrete variable that can take one of two values: +1 or -1 (interpreted as spin up or spin down). In ferromagnetic materials, spins tend to align with their neighbors to

minimize the system’s energy. The Ising model exhibits a phase transition at a critical temperature, below which spins align, resulting in net magnetization corresponding to the ferromagnetic phase. Above this temperature, thermal fluctuations dominate, and spins are randomly oriented, corresponding to the paramagnetic phase. BOOST-MI applies the Ising model to SRT data by treating spatial spots as spins, with the positive and negative values corresponding to high and low expression levels of a gene after dichotomization. BOOST-MI detects a gene as an overall SVG if it finds the gene to be in a “ferromagnetic phase.” BOOST-HMI extends this approach for imaging-based SRT data to accommodate the irregular spatial distribution of measured spots.

3.2 Graph-based methods

In manifold learning, when data originate from a non-linear manifold within Euclidean space, using a graph to represent the data effectively captures the intrinsic geometry and preserves the local structures of the manifold. Extending this concept to spatial spots on a non-linear manifold within the 2D Euclidean space of a tissue slice, graph-based SVG detection methods first construct a neighborhood graph by connecting nearby spots in Euclidean space. These methods then operate on the graph to detect overall SVGs. The way the graph is constructed is crucial, as it determines how well the graph represents the manifold, significantly impacting the performance of graph-based methods.

In this section, we introduce nine graph-based methods (Fig. 4), focusing on their graph construction approaches and subsequent operations on the graph for detecting overall SVGs.

Hotspot [40] aims to detect overall SVGs as the genes that exhibit high expression levels in local spot neighborhoods (i.e., “hotspots”). It first constructs a K -nearest neighbor (KNN) directed graph by treating each spot as a node and connecting it to its closest K spots in Euclidean distance. For a spot i connected to a spot j , with Euclidean distance denoted by d_{ij} , the directed edge from i to j is assigned a weight defined as $w_{ij} = e^{-d_{ij}^2/\sigma_i^2}$, where σ_i represents the bandwidth of spot i (defined as the distance from spot i to its $[K/3]$ -th neighbor). Next, for each gene, denoting its expression count at spot i by Y_i , Hotspot uses an autocorrelation statistic H to quantify the dependence of the gene’s expression level on the graph structure:

$$H = \sum_i \sum_{j \neq i} w_{ij} Y_i Y_j,$$

which is proportional to Moran’s I [36], a spatial autocorrelation measure that quantifies the degree to which similar expression levels are clustered together in space. Moran’s I is defined as

$$I = \frac{n}{\sum_i \sum_j w_{ij}} \frac{\sum_i \sum_j w_{ij} (Y_i - \bar{Y})(Y_j - \bar{Y})}{\sum_i (Y_i - \bar{Y})^2}, \quad (3.1)$$

where n is the number of spatial spots, and \bar{Y} is the gene’s mean expression level across spots. Similar to I , a large H indicates that spots where the gene is highly expressed are clustered in local

neighborhoods, suggesting the gene is an overall SVG. To assess the statistical significance of H , Hotspot converts H to a z-statistic by subtracting the expectation of H under the null model, where all spots are assumed to be independent, and dividing by the standard deviation of H under the null model. Specifically, Hotspot assumes two null models where Y_i independently follows either an NB distribution or a Bernoulli distribution. The z-statistic is then assumed to follow a standard Gaussian distribution under the null hypothesis, and a one-sided p-value is computed.

HRG [41] differs from Hotspot in three key aspects. First, it replaces the KNN graph with a shared-nearest-neighbors (SNN) graph, where the edge weight w_{ij} between spots i and j is defined as the Jaccard index of their respective K -nearest neighbors. The Jaccard index is calculated as the size of the intersection of the two sets divided by the size of their union. Second, HRG modifies Y_i , the gene count at spot i , to a z-score $Z_i = \frac{Y_i - \bar{Y}}{\sqrt{\frac{1}{n} \sum_{j=1}^n (Y_j - \bar{Y})^2}}$, where \bar{Y} is the mean gene count and n is the total number of spots. Third, unlike Hotspot, HRG does not provide statistical significance for its detected overall SVGs but instead ranks the genes based on H .

SVGbit [42] is also a spatial-autocorrelation-based method that ranks genes as overall SVGs based on the spatial autocorrelations of local neighborhoods. The method does not provide statistical significance for its rankings. For each gene, SVGbit uses three steps to calculate a summary statistic, called the “aggregation index,” which is used to rank genes. First, SVGbit identifies “hotspots” as spatial spots with large and statistically significant local Moran’s I values, using a z-test-based p-value thresholded at the 5% FDR. Specifically, for spot i , local Moran’s I is defined as

$$I_i = (Y_i - \bar{Y}) \sum_j w_{ij} (Y_j - \bar{Y}),$$

where the terms are defined similarly to Moran’s I (3.1). A high I_i value indicates that spot i is part of a neighborhood of similar values (either high-high or low-low). Hence, spot i is treated as a hotspot if I_i is deemed significantly large. Second, for each hotspot, SVGbit considers its neighboring hotspots among the 6-nearest-neighbor spots and defines the “local aggregation density” as the sum of these neighboring hotspots’ normalized log-transformed p-values (i.e., the log-transformed p-value of each neighboring hotspot divided by the sum of the log-transformed p-values of the 6 neighboring spots). Thus, a hotspot with more neighboring hotspots has a higher local aggregation density. Third, the gene’s aggregation index is computed as the average of all hotspots’ local aggregation densities. Intuitively, the overall SVGs with large aggregation indices are those whose expression patterns exhibit clustered hotspots.

SINFONIA [43] aims to detect overall SVGs as those exhibiting positive spatial autocorrelations, where similar expression levels are clustered in neighboring spots, either globally or locally. It begins by constructing a KNN directed graph, setting the edge weight from spot i to spot j (if connected) as $w_{ij} = 1 - \frac{d_{ij}}{\max_j d_{ij}}$, where d_{ij} is the Euclidean distance between spots i and j , and $\max_j d_{ij}$ is the maximum distance between spot i and its K nearest neighbors. Given this graph, SINFONIA calculates two measures of spatial autocorrelation for each gene: (1) Moran’s I [36], which provides a global measure of spatial autocorrelation, with values ranging from -1 to 1 ,

where a value close to 1 indicates strong positive spatial autocorrelation; (2) Geary's C [44], which is more sensitive to local spatial differences, with values ranging from 0 to 2, where a value close to 0 indicates strong positive spatial autocorrelation. Geary's C is defined as

$$C = \frac{(n - 1) \sum_i \sum_j w_{ij} (Y_i - Y_j)^2}{2 \sum_i \sum_j w_{ij} \sum_i (Y_i - \bar{Y})^2},$$

where the terms are defined similarly to Moran's I (3.1). SINFONIA then ranks genes from high to low based on Moran's I and from low to high based on Geary's C. To identify overall SVGs, SINFONIA takes the union of the top J genes from both rank lists, where J is a pre-specified positive integer. However, SINFONIA does not provide statistical significance for the detected overall SVGs.

MERINGUE [45] also uses Moran's I to detect overall SVGs but differs from previous methods in its graph construction approach. Instead of using a KNN graph, MERINGUE constructs a graph of spatial spots using Delaunay triangulation, making it suited for spatial spots with non-uniform density, such as cells in MERFISH data. Delaunay triangulation [46] connects points in a 2D space to form triangles such that no point lies inside the circumcircle (the circle that passes through all three vertices) of any triangle. In simpler terms, it maximizes the minimum angle of the triangles, avoiding skinny triangles. Unlike KNN, Delaunay triangulation does not require selecting an arbitrary K parameter and automatically adapts to variations in point density, providing more connections in denser regions and fewer in sparser regions. Given the graph, MERINGUE assigns an edge weight between spots i and j as $w_{ij} = 1$ if the two spots are connected, and $w_{ij} = 0$ otherwise. To determine if a gene is an overall SVG, MERINGUE uses Moran's I, transforms it to a z-statistic, and calculates a one-sided p-value based on a standard Gaussian distribution.

SpaGene [47], similar to previous methods that use Moran's I, aims to detect overall SVGs as those highly expressed at neighboring spots. Starting from a KNN graph of spots, it uses an alternative approach to boost computational efficiency. For each gene, it dichotomizes spots, coding them as 0 or 1 corresponding to low or high expression levels of the gene. It then extracts the high-expression spots (i.e., the spots labeled as 1) from the graph and summarizes the distribution of these spots' degrees (the number of edges connected to each spot) in the subgraph. Finally, it compares the degree distribution of these high-expression spots to that of the whole graph, and calculates the earth mover's distance between the two distributions. A small distance indicates that the high-expression spots are densely connected to each other and rarely connected to other spots, so the gene is likely an overall SVG. Finally, SpaGene converts the distance to a p-value using a permutation test.

BinSpect, part of the Giotto toolbox [48], detects overall SVGs by examining whether the dichotomized spots (i.e., spots coded as 0 or 1 corresponding to low and high expression levels of a gene, respectively) are randomly distributed in a graph. Specifically, BinSpect constructs a graph of spots either as a KNN graph or by Delaunay triangulation. Then, for each gene, BinSpect follows three steps to determine if the gene is an overall SVG. First, it assigns a binary label

to each spot by either thresholding at the top 30% expressed spots or using k -means clustering ($k = 2$). Second, it constructs a 2-by-2 contingency table by counting the edges that connect spots with labels (0,0), (0,1), (1,0), or (1,1). Finally, it applies Fisher's exact test to the contingency table to decide whether spots with the same label tend to be connected, thereby detecting a gene as an overall SVG.

Note that, unlike Giotto, two other popular single-cell toolkits with SRT functionalities, Seurat [49] and squidpy [50], use Moran's I to detect overall SVGs.

scGCO [51] is similar to BinSpect at a high level by testing whether a gene's discretized expression levels are dependent on spatial neighborhoods. However, scGCO approaches the problem in a more complex way. After constructing an undirected graph of spots using Delaunay triangulation, scGCO performs three steps. First, it fits a Gaussian mixture model to the gene's log-transformed expression levels to discretize the gene's expression into a number of levels. Second, using a graph cut algorithm, it fits a hidden Markov random field to the gene's log-transformed expression levels on the spot graph to divide the spots into segments. Finally, it tests whether each discretized level is randomly distributed in each segment, using the homogeneous Poisson process as the underlying null model. In summary, a gene is considered an overall SVG if at least one of its discretized levels is non-randomly distributed in any segment.

RayleighSelection [52] is a theoretical approach that generalizes a graph to a simplicial complex [53], incorporating additional higher-dimensional topological information about spatial spots compared to a graph. The method first constructs the Vietoris-Rips complex, a type of simplicial complex, of spatial spots by considering balls of a fixed radius around each spot and forming edges, triangles, and higher-dimensional simplices based on the intersections of these balls. For each gene, it then computes the combinatorial Laplacian score, which measures how well the gene respects the local structure of the simplicial complex. If a gene has high expression levels in highly connected regions, it will have a low combinatorial Laplacian score, indicating a significant spatial pattern and suggesting it to be an overall SVG. Finally, RayleighSelection computes a p-value for the combinatorial Laplacian score using a permutation test.

3.3 Relationship between Euclidean-space-based methods and graph-based methods

When it is reasonable to assume data lie on a non-linear manifold in Euclidean space, using a graph to represent the data offers significant advantages. A graph can capture the intrinsic geometry of the manifold by representing data points as nodes and their similarity relationships as edges based on some similarity or distance measure. Graph-construction methods like KNN (where each node's neighborhood is defined by a fixed number of neighbors, K) or ϵ -neighborhoods (where each node's neighborhood is defined by a fixed radius, ϵ) ensure that each node is connected to its nearest neighbors, preserving the local relationships among nodes. The shortest-path distance between two nodes in the graph approximates their "geodesic distance" on the manifold, reflecting

the data’s intrinsic structure more accurately than Euclidean distances. Additionally, graph-based methods are more robust to the curse of dimensionality: in high-dimensional spaces, where Euclidean distances often lose meaning, a graph can effectively capture relationships among data points.

However, in the context of SVG detection, using Euclidean distance to represent distances between spots might be more appropriate. Biological relationships between spots inherently follow Euclidean distances in a physical 2D Euclidean space in tissue. Moreover, since Euclidean distances are based on 2D spatial locations rather than high-dimensional gene expression data, the curse of dimensionality is not an issue.

It remains an open question how to construct a graph to accurately represent a non-linear manifold of spatial spots. The choice of graph-construction method, such as KNN or Delaunay triangulation, is crucial. KNN connects each spot to its K nearest neighbors, preserving the local structure of the data. In contrast, Delaunay triangulation handles the non-uniform spatial distribution of spots in SRT data, such as MERFISH or Slide-seq data. Delaunay triangulation connects spots to form triangles such that no point is inside the circumcircle of any triangle, resulting in a graph that more naturally respects the non-uniform distribution of spots and preserves local density variations. However, Delaunay triangulation is more computationally expensive and more sensitive to outliers than KNN.

Additionally, the definition of edge weights in the graph is another important consideration. Edges can be directional or undirectional, depending on whether the relationship between spots has a direction (e.g., one cell type influencing another cell type’s gene expression). The edge weights can take multiple forms. For example, weights can be determined by a Gaussian kernel, where weights decay exponentially with the Euclidean distance between spots, emphasizing closer spots. Alternatively, weights can decrease linearly with distance. These choices affect how the graph captures the manifold structure of data and, consequently, how effectively it can be used to detect spatial patterns of gene expression that are biologically relevant.

4 Methods for detecting cell-type-specific SVGs

In both sequencing- and imaging-based SRT data, a gene’s expression variance across spots can result from the gene’s different expression levels in distinct cell types. Given that cell types are typically distributed non-uniformly in the tissue slice, neglecting the cell type information of spatial spots may prevent the discovery of SVGs that are purely driven by spatial locations [54, 55]. Thus, we define *cell-type-specific SVGs* as the category of SVGs detected using both SRT data and external cell-type annotations for the spatial spots (Fig. 2). Unlike the methods for detecting overall SVGs that do not consider cell type annotations, the three methods for detecting cell-type-specific SVGs—CTSV [54], C-SIDE [56], and spVC [57]—begin by annotating the cell types of the spatial spots in SRT data and then use a regression framework to identify SVGs within cell types by examining the interaction effects between cell types and spatial locations (see Section 7.2.1 for

a detailed discussion on the general framework).

CTSV assumes a ZINB distribution for a given gene's expression count Y_i at spot i :

$$Y_i \stackrel{\text{ind}}{\sim} \text{ZINB}(\mu_i(\mathbf{s}_i), \boldsymbol{\theta}),$$

where $\mu_i(\mathbf{s}_i)$ is the mean expression function of the spatial location $\mathbf{s}_i = (s_{i1}, s_{i2})$, and $\boldsymbol{\theta}$ indicates the other parameters (dispersion and zero-inflated probability) necessary to describe the distribution. To determine if the gene is a cell-type-specific SVG, CTSV includes K cell types' cell-type-level mean functions of \mathbf{s}_i : $\eta_k(\mathbf{s}_i)$, $k = 1, \dots, K$, and assumes that

$$\begin{aligned} \log \mu_i(\mathbf{s}_i) &= \log \ell_i + \sum_{k=1}^K \eta_k(\mathbf{s}_i) w_{ik}, \\ \eta_k(\mathbf{s}_i) &= \beta_{k0} + \beta_{k1} b_1(s_{i1}) + \beta_{k2} b_2(s_{i2}). \end{aligned}$$

where weights w_{ik} , $k = 1, \dots, K$, are pre-estimated cell type proportions of spot i obtained by spatial deconvolution methods such as SPOTlight [58] and RCTD [55], and $b_1(s_{i1})$ and $b_2(s_{i2})$ are two non-cell-type-specific, non-parametric, univariate functions of the spatial coordinates in the two dimensions. CTSV then tests if β_{k1} and β_{k2} are both zero. If not, the gene is considered an SVG specific to cell type k .

C-SIDE is similar to CTSV but has three major differences. First, C-SIDE assumes a Poisson distribution for Y_i . Second, C-SIDE assumes a different relationship between $\mu_i(\mathbf{s}_i)$ and $\eta_k(\mathbf{s}_i)$, $k = 1, \dots, K$. Third, C-SIDE uses a different non-parametric function form for each $\eta_k(\mathbf{s}_i)$.

$$\begin{aligned} Y_i &\stackrel{\text{ind}}{\sim} \text{Poisson}(\mu_i(\mathbf{s}_i)), \\ \log(\mu_i(\mathbf{s}_i)) &= \gamma_0 + \log \ell_i + \log \left(\sum_{k=1}^K \eta_k(\mathbf{s}_i) w_{ik} \right) + \varepsilon_i, \\ \log(\eta_k(\mathbf{s}_i)) &= \beta_{k0} + \sum_{\ell=1}^L \beta_{k\ell} b_\ell(\mathbf{s}_i), \end{aligned}$$

where the common terms are defined similarly to CTSV, ε_i is a zero-mean random-effect term, and $\sum_{\ell=1}^L \beta_{k\ell} b_\ell(\mathbf{s}_i)$ is a non-cell-type-specific, bivariate smooth-spline function of \mathbf{s}_i consisting of L basis functions. C-SIDE then tests if $\beta_{k1}, \dots, \beta_{kL}$ are all zero. If not, the gene is considered an SVG specific to cell type k .

spVC is similar to C-SIDE but assumes a different relationship between $\mu_i(\mathbf{s}_i)$ and $\eta_k(\mathbf{s}_i)$, $k = 1, \dots, K$.

$$\log(\mu_i(\mathbf{s}_i)) = \gamma_0 + \log \ell_i + \sum_{k=1}^K w_{ik} \beta_k + \sum_{k=1}^K \eta_k(\mathbf{s}_i) w_{ik} + \gamma(\mathbf{s}_i),$$

which considers cell types' non-spatial effects as $\sum_{k=1}^K w_{ik} \beta_k$ and a baseline spatial effect $\gamma(\mathbf{s}_i)$.

Then, spVC implements a two-step testing procedure. First, it tests whether β_1, \dots, β_K are all zero and whether $\gamma(\cdot) = 0$ in a reduced model without the cell-type-specific spatial effect term $\sum_{k=1}^K \eta_k(\mathbf{s}_i) w_{ik}$. If both null hypotheses are rejected, the second step is to test whether $\eta_k(\cdot) = 0$. If not, the gene is considered a SVG specific to cell type k .

5 Methods for detecting spatial-domain-marker SVGs

We define *spatial-domain-marker SVGs* as the category of SVGs detected using SRT data and spatial domains derived from the same data (Fig. 2). Unlike previous SVG detection methods, the two methods for detecting spatial-domain-marker SVGs—**SpaGCN** [59] and **DESpace** [60]—first partition spatial spots into more than one spatial domain. Then, they implement hypothesis tests to assess a gene’s mean expression differences between these spatial domains. A gene is defined as a marker SVG of a spatial domain if it is significantly more highly expressed in that domain than in other domains.

SpaGCN identifies spatial domains using a pre-trained graph convolutional network applied to SRT data and the paired H&E image. For each gene, it performs Wilcoxon rank-sum tests on normalized expression levels between each domain and the neighboring spots. If the gene is found to be significantly highly expressed in a domain, it is considered a marker SVG of that domain.

DESpace first implements existing spatial clustering methods, such as BayesSpace [61] and StLearn [62], on SRT data to identify spatial clusters as spatial domains. Then, for each gene, DESpace uses an NB generalized linear model to assess if the spatial domains have a significant effect on the gene’s expression. If so, the gene is identified as a spatial-domain-marker SVG associated with the domain in which it is significantly more highly expressed than in other domains.

6 Applications of SVGs

The three categories of SVG detection methods have different goals. Overall SVG detection screens informative genes for downstream analysis, such as spatial domain identification. Cell-type-specific SVG detection reflects spatial variation within a cell type, aiding in the understanding of cell-type-level spatial gene expression. Spatial-domain-marker SVG detection is used to find marker genes to annotate and interpret spatial domains already detected.

6.1 Application of overall SVGs for spatial domain identification

The detection of overall SVGs serves as a pre-processing step in SRT data analysis. While the definition of overall SVGs may vary across methods, the common objective is to select informative genes for downstream analysis. A common downstream analysis is to identify *spatial domains*

(also referred to as *spatial communities*) by partitioning a tissue slice into regions so that spots have similar expression profiles of overall SVGs in each region.

Identifying spatial domains can help uncover tissue layers where morphological architecture is less defined. For example, SPADE [37], an overall SVG detection method, uses its detected overall SVGs to identify spatial domains as substructures in cortical layers and amygdala in a 10x Visium mouse brain immunofluorescence dataset. Another use of spatial domain identification is to reveal gene expression profiles underlying tissue structures. For example, scGCO [63], another overall SVG detection method, identifies spatial domains from a mouse breast cancer biopsy dataset sequenced by Spatial Transcriptomics [64], and the identified domains align with annotated tissue structures including invasive ductal cancer, ductal cancer, and normal tissue. This alignment confirms that these tissue structures have distinct gene expression profiles, so the SRT data can potentially lead to the discovery of new marker genes for these tissue structures, a task tackled by spatial-domain-marker SVG detection.

A common approach to identifying spatial domains is clustering spatial spots using overall SVGs' expression levels and spot locations. For example, graph-based clustering (e.g., Louvain clustering) can be applied after spatial spots are connected into a graph based on their spatial proximity and gene expression levels; then, the identified clusters contain spatial spots in proximity and exhibiting similar gene expression levels. For example, using Louvain clustering, two overall SVG detection methods, SPADE [37] and SINFONIA [43], identify spatial domains in well-structured brain tissues in the mouse olfactory bulb Spatial Transcriptomics dataset [64] and the mouse hippocampus seqFISH [5] and Slide-seq [65] dataset.

The spatial domains identified from overall SVGs can be validated, directly or indirectly, in three ways. First, spatial domains can be compared with tissue layers annotated by pathologists from the H&E image accompanying the SRT data (e.g., 10x Visium). For example, in the SpaGCN [59] method paper, three annotated layers of the primary pancreatic cancer were compared to the spatial domains identified from a Spatial Transcriptomics dataset [66]. Second, spatial domains can be annotated with cell-type labels in external transcriptomic data to verify if distinct domains have different cell-type compositions. For example, in a study of the human dorsolateral prefrontal cortex 10x Visium dataset [67], researchers annotated the identified spatial domains as cortical layers based on the cytoarchitecture and marker genes obtained from external large-scale single nucleus RNA-seq datasets. Third, for a well-structured tissue type, such as the brain, spatial domains can be annotated by transferring tissue layer labels from external public annotations so that spatial domains, if reasonable, can be annotated as tissue layers confidently. For instance, in the SINFONIA [43] method paper, annotations from Allen Brain Atlas [68] and Mouse Brain Gene Expression Atlas (<http://mousebrain.org/>) were transferred to several SRT datasets, including the mouse brain coronal section 10x Visium dataset, the mouse hippocampus Slide-seqV2 dataset [65], and the mouse olfactory bulb STEREO-seq dataset [14].

6.2 Applications of cell-type-specific SVGs

Although not specified by existing cell-type-specific SVG detection methods, potential applications of cell-type-specific SVGs include two directions. First, by examining the expression patterns of the SVGs within specific cell types, researchers can gain insights into the effects of spatial locations and interactions with other cell types. Second, cell-type-specific SVGs can be used to identify and characterize distinct cell subpopulations or states within cell types, with the potential to advance our knowledge of cellular behavior in a spatial context.

6.3 Applications of spatial-domain-marker SVGs

Characterizing spatial domains in a tissue slice, spatial-domain-marker SVGs have two potential applications. First, they help understand the underlying molecular mechanisms of spatial domains when the domains align with tissue structures. Second, they assist in annotating tissue layers in other datasets. For example, in the SpaGCN [59] method paper, it was demonstrated that the spatial-domain-marker SVGs detected by SpaGCN from a LIBD human dorsolateral prefrontal cortex slice (No. 151673) could be used to identify the same layers in another slice (No. 151507) of a different brain.

7 Theoretical characterization of SVG detection methods that use frequentist hypothesis tests

Among the 31 SVG detection methods, 21 of them implement statistical hypothesis tests to detect SVGs using *frequentist inference* (i.e., defining a test statistic, deriving the test statistic's null distribution, and converting the test statistic value to a p-value). For these frequentist hypothesis-testing-based methods, their null and alternative hypotheses direct their SVG detection. In general, methods that use different null hypotheses are not directly comparable. The reason is that a gene may satisfy one null hypothesis (and is a true non-SVG) but not the other null hypothesis (and is a true SVG). Hence, we would like to clarify and categorize the null hypotheses used in the 21 methods to deepen our understanding of these methods' conceptual similarities and differences.

Based on the types of null hypotheses, in Table 1 we summarize the hypothesis tests used in the 21 methods into three types: dependence tests, regression fixed-effect tests, and regression random-effect tests (also known as variance component tests). So far, dependence tests and regression random-effect tests have only been used for overall SVG detection, while regression random-effect tests have been used to detect all three categories of SVGs. For each method, besides the test type, we also list the test statistic and null distribution in Table 3.

Among the three types of hypothesis tests for SVG detection, dependence tests have the most general null hypothesis: a gene's expression level is independent of the spatial location. In contrast, the two types of regression tests rely on specific assumptions for a regression model,

which has a gene’s expression level as the response variable and the spatial location as the predictor (also known as the covariate or explanatory variable). The co-existence of dependence tests and model-specific regression tests is common in the statistics literature [69]. In general, dependence tests, thanks to their general independence null hypothesis, can capture SVGs with more diverse patterns but can be less powerful for detecting SVGs of specific patterns, compared to the regression tests. In contrast, relying on specific model assumptions, regression tests are more powerful for discovering the SVGs satisfying the assumptions but, meanwhile, more prone to false discoveries when the model assumptions do not hold [70]. It remains an open question to benchmark the three types of tests regarding robustness to model misspecification and the trade-off between robustness and power. Additionally, it is important to identify which assumptions are more reasonable for SRT data generated from various tissues and by different technologies.

7.1 Dependence tests

For a given gene, the most general hypothesis test for SVG detection is to decide whether the gene’s expression level Y is independent of the spatial location S , i.e., the null hypothesis is

$$H_0 : Y \perp S.$$

In this formulation, we assume that $(y_1, s_1), \dots, (y_n, s_n)$ are independently sampled from the joint distribution of (Y, S) , where (y_i, s_i) indicates spot i ’s expression level of the given gene and spatial location. When the independent null hypothesis H_0 holds, the gene is a *true overall SVG*.

Out of the 21 frequentist hypothesis-testing-based SVG detection methods, nine methods adopt the dependent test formulation, constructing a test statistic to summarize the dependence between a gene’s expression level and the spatial location. The nine methods are SPARK-X, Trendsceek, singlecellHaystack, Hotspot, MERINGUE, BinSpect, scGCO, RayleighSelection, and SpaGene. We categorize the test statistics used in the nine methods into two types: conventional test statistics with theoretical null distributions (SPARK-X, Hotspot, MERINGUE, BinSpect, and scGCO) and unconventional test statistics with permutation-based null distributions (Trendsceek, singlecellHaystack, RayleighSelection, and SpaGene).

Among the five methods that use conventional test statistics with theoretical null distributions, SPARK-X is a representative method [28]. The SPARK-X test statistic is defined to capture the “agreement” between two spot similarity matrices (referred to as “covariance matrices” by the SPARK-X authors), one defined based on a gene’s expression levels at the n spots and the other based on the spatial locations of the n spots (subject to a transformation of the locations before defining the similarity between spots, so that the similarity matrix reflects a specific spatial pattern such as Gaussian and cosine kernels). Specifically, the test statistic is defined as $(1/n)$ times the trace of the product of the two similarity matrices. The rationale is that under the independence null hypothesis, the test statistic should be small and follow a theoretical, asymptotic null distribution as a mixture chi-square distribution.

The four methods that use unconventional test statistics generate the null distribution by permuting a gene's expression levels across the n spots, thus removing any dependence between the gene's expression level and the spatial location. The permutation procedure is a general solution for obtaining the null distribution when the theoretical null distribution is difficult to derive, but it is computationally intensive due to the need for repetitive permutations to generate the null distribution. For example, singlecellHaystack [29] defines a test statistic based on the KL divergence of the conditional density of spots' spatial locations, which is conditional on a gene's dichotomized expression level (on or off), from the unconditional density of spots' spatial locations. Specifically, both densities are defined for each spatial grid, which consists of many spots and is pre-defined by the singlecellHaystack algorithm. Then, the test statistic is a summation of the KL-divergence-like statistics across the spatial grids. As this test statistic is complex and has no theoretical null distribution, the permutation is used to generate the null distribution.

7.2 Regression tests

There are two types of regression tests: fixed-effect tests, where the effect of the spatial location is assumed to be fixed, and random-effect tests, which assume the effect of the spatial location as random. To explain these two types of tests, we start with a *linear mixed model* for a given gene

$$Y_i = \beta_0 + \mathbf{x}_i^\top \boldsymbol{\beta} + \mathbf{z}_i^\top \boldsymbol{\gamma} + \epsilon_i, \quad (7.1)$$

where the response variable Y_i is the gene's expression level at spot i , $\mathbf{x}_i \in \mathbb{R}^p$ indicates the fixed-effect covariates of spot i , $\mathbf{z}_i \in \mathbb{R}^q$ denotes the random-effect covariates of spot i , and ϵ_i is the random measurement error at spot i with $\mathbb{E}[\epsilon_i] = 0$. In the model parameters, β_0 is the (fixed) intercept, $\boldsymbol{\beta} \in \mathbb{R}^p$ indicates the fixed effects, and $\boldsymbol{\gamma} \in \mathbb{R}^q$ denotes the random effects with zero means $\mathbb{E}[\boldsymbol{\gamma}] = 0$ and the covariance matrix $\text{Var}(\boldsymbol{\gamma}) = \boldsymbol{\Sigma} \in \mathbb{R}^{q \times q}$. In this linear mixed model, independence is assumed between $\boldsymbol{\gamma}$ and $\boldsymbol{\epsilon} = (\epsilon_1, \dots, \epsilon_n)^\top$ and among $\epsilon_1, \dots, \epsilon_n$.

Fixed-effect tests examine whether some or all of the fixed-effect covariates \mathbf{x}_i contribute to the mean of the response variable $\mathbb{E}[Y_i]$. If all fixed-effect covariates make no contribution, then $\mathbb{E}[Y_i | \mathbf{x}_i] = \mathbb{E}[Y_i]$. The null hypothesis

$$H_0 : \boldsymbol{\beta} = \mathbf{0},$$

implies $\mathbb{E}[Y_i | \mathbf{x}_i] = \mathbb{E}[Y_i]$, $i = 1, \dots, n$.

Random-effect tests examine whether the random-effect covariates contribute to the variance of the response variable $\text{Var}(Y_i)$, focusing on the decomposition

$$\text{Var}(Y_i) = \text{Var}(\mathbb{E}[Y_i | \mathbf{z}_i]) + \mathbb{E}[\text{Var}(Y_i | \mathbf{z}_i)] = \mathbf{z}_i^\top \boldsymbol{\Sigma} \mathbf{z}_i + \text{Var}(\epsilon_i) \quad (7.2)$$

and testing if the contribution of the random-effect covariates $\text{Var}(\mathbb{E}[Y_i | \mathbf{z}_i])$ is zero. The null hypothesis

$$H_0 : \boldsymbol{\Sigma} = \mathbf{0}$$

implies $\text{Var}(\mathbb{E}[Y_i|\mathbf{z}_i]) = 0, i = 1, \dots, n$.

To generalize the linear mixed model (7.1) for data where the response variable Y_i is not continuous (e.g., binary or count), we can decompose the model into a *random structure*, where each Y_i independently follows a distribution with mean $\mu_i = \mathbb{E}[Y_i]$, and a *systematic structure* that links μ_i to the fixed-effect covariates \mathbf{x}_i . Specifically, for the model (7.1), if we assume that $\boldsymbol{\gamma} \sim N(\mathbf{0}, \boldsymbol{\Sigma})$ and $\epsilon_i \sim N(0, \sigma^2)$, then the *random structure* is

$$Y_i \stackrel{\text{ind}}{\sim} N(\mu_i, \mathbf{z}_i^\top \boldsymbol{\Sigma} \mathbf{z}_i + \sigma^2),$$

and the *systematic structure* is

$$\mu_i = \beta_0 + \mathbf{x}_i^\top \boldsymbol{\beta}.$$

The generalization of the linear mixed model can occur in both the random and systematic structures. For simplicity, we only focus on the fixed-effect covariates \mathbf{x}_i for the generalization and omit the random-effect covariates \mathbf{z}_i . If we change the random structure from the Gaussian distribution to another exponential-family distribution,

$$Y_i \stackrel{\text{ind}}{\sim} \text{Exponential Family}(\mu_i, \phi), \quad (7.3)$$

where ϕ is a nuisance parameter not of primary interest. An example of exponential-family distribution is the Poisson distribution $Y_i \sim \text{Poisson}(\mu_i)$. According to the random structure change, the systematic structure can be written in general as

$$g(\mu_i) = \beta_0 + \mathbf{x}_i^\top \boldsymbol{\beta}, \quad (7.4)$$

where the function $g(\cdot)$ is referred to as the *link function* and specified based on the distribution in the random structure. We refer to the model specified by (7.3)–(7.4) as a *generalized linear model*. If we further generalize the systematic structure so that the effects of the p covariates in $\mathbf{x}_i = (x_{i1}, \dots, x_{ip})^\top$ on μ_i is non-linear and additive:

$$g(\mu_i) = \beta_0 + \sum_{j=1}^p f_j(x_{ij}), \quad (7.5)$$

we referred to the model specified by (7.3) and (7.5) as a *generalized additive model*.

For regression models with different complexities (roughly speaking, different numbers of parameters to estimate), model selection centers on the bias-variance trade-off. An oversimplified model misses key data characteristics, leading to biased parameter estimates, though with low variance. In contrast, an overly complex model wastes parameters on unimportant details, increasing variance in parameter estimates. As a trade-off, a reasonable model appropriately addresses the data characteristics without overfitting the data noise, thereby being more powerful and robust.

For SVG detection, the effect of the spatial location \mathbf{s}_i on the given gene's expression level Y_i

can be formulated as either fixed or random. In the following two subsections, we will discuss the SVG detection methods that adopt each formulation.

7.2.1 Regression fixed-effect tests

Among the 21 frequentist hypothesis-testing-based SVG detection methods, six methods use the regression fixed-effect test formulation: SPADE, C-SIDE, CTSV, spVC, SpaGCN, and DESpace. Notably, unlike dependence tests and regression random-effect tests, only regression fixed-effect tests cover all three SVG categories: overall SVGs, cell-type-specific SVGs, and spatial-domain-marker SVGs. Methods within each category use the same fixed-effect covariates \mathbf{x}_i for spot i , while methods of different categories use different \mathbf{x}_i 's. Below, we introduce the six methods in the three categories.

For overall SVG detection, SPADE [37] is the only method that detects overall SVGs. For a given gene, it uses a linear model without random-effect covariates:

$$\mu_i = \beta_0 + \mathbf{x}_i(\mathbf{s})^\top \boldsymbol{\beta},$$

where the fixed-effect covariates $\mathbf{x}_i(\mathbf{s})$ are defined as some processed features from the n spots' spatial locations \mathbf{s} and an H&E image. Specifically, the processed features are based on 512 features from a pre-trained convolutional neural network applied to an H&E image. The gene is a *true overall SVG* if $\boldsymbol{\beta} \neq 0$. SPADE uses the R package limma [71] to fit the linear model and tests if each component of $\boldsymbol{\beta}$ is zero using a t test.

For cell-type-specific SVG detection, the fixed-effect covariates of spot i (i.e., \mathbf{x}_i) include the library size ℓ_i (i.e., spot i 's total expression count), the cell type $\mathbf{c}_i = (c_{i1}, \dots, c_{iK})^\top \in [0, 1]^K$, and the spatial location $\mathbf{s}_i \in \mathbb{R}^2$ (see Section 2 for definitions). The considered fixed effects include the marginal effects of \mathbf{c}_i and \mathbf{s}_i and their interactive effects. Hence, in a generalized additive model formulation for a given gene, the systematic structure is

$$g(\mu_i) = \beta_0 + \log \ell_i + \sum_{k=1}^K c_{ik} \beta_k + f_0(\mathbf{s}_i) + \sum_{k=1}^K c_{ik} f_k(\mathbf{s}_i), \quad (7.6)$$

where β_0 is the overall intercept, $\log \ell_i$ is the intercept effect of spot i 's library size, β_k indicates the cell-type-specific spatial-invariant effect for cell type k , $f_0(\mathbf{s}_i)$ is the overall spatial effect at spot i , and $f_k(\mathbf{s}_i)$ is the cell-type-specific spatial effect for cell type k at spot i . For identifiability, constraints are needed for $\boldsymbol{\beta} = (\beta_1, \dots, \beta_K)^\top$ and $f_0(\cdot), f_1(\cdot), \dots, f_K(\cdot)$. The gene is a *true cell-type-specific SVG* of cell type k if $f_k(\cdot) \neq 0$.

C-SIDE, CTSV, and spCV are three methods for cell-type-specific SVG detection. As an example method, spVC [57] assumes a gene's expression count Y_i follows a Poisson distribution (i.e., the random structure (7.3)) with the systematic structure (7.6). To decide whether the gene is a cell-type-specific SVG, spVC implements a two-step procedure for sequential hypothesis tests. First, it considers a reduced model without interactive effects between \mathbf{c}_i and \mathbf{s}_i , so the systematic

structure becomes

$$g(\mu_i) = \beta_0 + \log \ell_i + \sum_{k=1}^K c_{ik} \beta_k + f_0(\mathbf{s}_i).$$

Then it tests two null hypotheses: $H_0 : \boldsymbol{\beta} = (\beta_1, \dots, \beta_K)^\top = \mathbf{0}$ and $H_0 : f_0(\cdot) = 0$ using the likelihood ratio test and the Wald test, respectively. If both null hypotheses are rejected, it proceeds to the second step. Second, it considers the full model with interactive effects, with the systematic structure (7.6). It tests if any of the interactive effects $f_1(\cdot), \dots, f_K(\cdot)$ are 0 using the likelihood ratio test. Similar to spVC, CTSV [54] assumes a generalized additive model. However, CTSV has a different random structure and testing procedure. Specifically, CTSV assumes the random structure to be that Y_i follows a ZINB distribution, and the systematic structure is written as

$$g(\mu_i) = \beta_0 + \log \ell_i + \sum_{k=1}^K c_{ik} \beta_k + \sum_{k=1}^K c_{ik} f_k(\mathbf{s}_i), \quad (7.7)$$

where $f_k(\mathbf{s}_i)$ is further assumed to be additive $f_k(\mathbf{s}_i) = f_{k1}(s_{i1}) + f_{k2}(s_{i2})$. Unlike spVC's two-step testing procedure, CTSV directly tests if any of the interactive effects $f_1(\cdot), \dots, f_K(\cdot)$ are 0 using the Wald test. Same as spVC, C-SIDE [56] assumes the random structure to be Poisson. However, it has a more complicated systematic structure than that of spVC and CTSV, allowing for random effects and additional non-linear transformations. C-SIDE uses a two-sided z-test.

For spatial-domain-marker SVG detection, the fixed-effect covariates of spot i (i.e., \mathbf{x}_i) include the library size ℓ_i and the spatial domain, indicated by $\mathbf{d}_i = (d_{i1}, \dots, d_{iL}) \in \{0, 1\}^L$, with $\sum_{l=1}^L d_{il} = 1$ (that is, $d_{il} = 1$ if spot i belongs to domain l). Then the systematic structure becomes

$$g(\mu_i) = \beta_0 + \log \ell_i + \sum_{l=1}^L d_{il} \beta_l, \quad (7.8)$$

where β_l indicates the effect of spatial domain l on $g(\mu_i)$, i.e., the transformed gene i 's true expression level. For identifiability, constraints are needed for $\boldsymbol{\beta} = (\beta_1, \dots, \beta_L)^\top$, e.g., $\beta_1 = 0$. The gene is a *true spatial-domain-marker SVG* (i.e., a DEG across spatial domains) if $\boldsymbol{\beta} \neq \mathbf{0}$.

SpaGCN and DESpace are two methods for spatial-domain-marker SVG detection. Following the systematic structure (7.8), DESpace [60] assumes the gene expression Y_i follows an NB distribution and tests the null hypothesis $H_0 : \boldsymbol{\beta} = \mathbf{0}$ using the likelihood ratio test statistic, which follows an asymptotic chi-square distribution under the null hypothesis. For SpaGCN [59], although it does not explicitly adopt a regression framework but instead uses the Wilcoxon rank-sum test on normalized gene expression levels (with the library size effect removed) to decide if a gene is more highly expressed in one spatial domain than its neighboring spots, the Wilcoxon rank-sum is a score test statistic of the proportional odds ordinal logistic regression model. Hence, the test in SpaGCN can broadly be considered to follow the systematic structure (7.8).

7.2.2 Regression random-effect tests

Unlike the nine methods that adopt dependence tests and the six methods that use regression fixed-effect tests, the last six of the 21 frequentist hypothesis-testing-based methods use regression random-effect tests: SpatialDE, nnSVG, SOMDE, SVCA, SPARK, and GPcounts.

All the six methods generalize the linear mixed model (7.1) for each gene, by encoding the spatial location \mathbf{s}_i of spot i as the random-effect covariate \mathbf{z}_i . With n spots, $\mathbf{z}_i = (z_{i1}, \dots, z_{in})^\top \in \{0, 1\}^n$ is a binary indicator vector with only one 1 indicating spot i . Without loss of generality, we assume that $z_{ii} = 1$. Then, the corresponding random-effect vector $\boldsymbol{\gamma} = (\gamma_1, \dots, \gamma_n)^\top \in \mathbb{R}^n$ has γ_i indicating the random effect of \mathbf{s}_i . The covariance matrix of $\gamma_1, \dots, \gamma_n$, $\text{Var}(\boldsymbol{\gamma})$, is assumed to depend on the spatial proximity of $\mathbf{s}_1, \dots, \mathbf{s}_n$. Accordingly, $\boldsymbol{\gamma}$ can be explicitly written as $\boldsymbol{\gamma}(\mathbf{s})$. When the null hypothesis $H_0 : \text{Var}(\boldsymbol{\gamma}(\mathbf{s})) = \mathbf{0}$ does not hold, the gene is a *true overall SVG*.

As an early and exemplar method, for each gene SpatialDE [20] assumes a linear random-effect model that only contains \mathbf{z}_i as the random-effect covariates:

$$Y_i = \beta_0 + \mathbf{z}_i^\top \boldsymbol{\gamma}(\mathbf{s}) + \epsilon_i, \quad (7.9)$$

where the random errors $\epsilon_1, \dots, \epsilon_n$ independently follow a Gaussian distribution $N(0, \delta)$, and the random effects $\boldsymbol{\gamma}(\mathbf{s})$ jointly follow a multivariate Gaussian distribution $\text{MVN}(\mathbf{0}, \sigma_s^2 \cdot \mathbf{K}(\mathbf{s}))$, with $\mathbf{K}(\mathbf{s}) = [K(\mathbf{s}_i, \mathbf{s}_j)]_{n \times n}$ specified by a kernel function $K(\cdot, \cdot)$ applied to the n spatial locations. This model is essentially a Gaussian process. The null hypothesis then becomes $H_0 : \sigma_s^2 = 0$.

Two methods, nnSVG [21] and SOMDE [23], also use the Gaussian process model as in SpatialDE but adopt more efficient computational algorithms. The other three methods extend the Gaussian process model. Specifically, SVCA [24] considers two additional variance terms to accommodate other covariates, such as cell-cell interactions. Instead of assuming that Y_i follows a Gaussian distribution, SPARK [25] and GPcounts [26] assume Poisson and NB distributions, respectively, and generalize the linear mixed effect model (7.9) to generalized linear mixed effect models.

All six methods use the likelihood ratio test with an asymptotic chi-square distribution under the null hypothesis.

8 Discussion and future directions

Below, we discuss the comparative advantages and trade-offs of existing SVG detection methods in terms of detection power, specificity, and scalability. Further, we outline two future directions for improving SVG detection methods: (1) accommodating various SRT technologies with distinct traits and (2) enhancing statistical rigor and method validation.

8.1 Power, specificity, and scalability of SVG detection methods

Among the 26 methods for detecting overall SVGs, the nine Euclidean-space-based, kernel-based methods define more specific spatial patterns for overall SVGs than the Euclidean-space-based, kernel-free methods and the graph-based methods. The statistical power of these kernel-based methods depends on the alignment between the pre-defined kernels' spatial patterns and the biologically relevant spatial patterns in SRT data. This alignment is often questionable because biologically relevant patterns are rarely as regular as the pre-defined kernel patterns. As a result, kernel-based methods may lose statistical power when this alignment is poor. To address this, some kernel-based methods, such as SPARK [25], incorporate multiple pre-defined kernels to capture a broader diversity of spatial patterns. Despite the potential loss of overall power, kernel-based methods are more specific and powerful for discovering overall SVGs whose spatial expression patterns align with the kernels compared to methods that do not use kernels. In short, there is a trade-off between overall power and specificity: methods targeting specific spatial patterns are less powerful at discovering other patterns, leading to a loss of overall power, but more powerful at discovering the targeted patterns with higher specificity.

Four types of genes that exhibit interesting but non-global expression patterns can be easily missed by methods that detect overall SVGs. First, some genes of interest may only be highly expressed in small regions of interest (ROIs) and can be overlooked by methods that do not distinguish small ROIs. For such genes, methods that detect spatial-domain-marker SVGs, such as SpaGCN [59], might be more appropriate because these methods can identify small ROIs as spatial domains in the first step before identifying marker genes in the second step. Second, there are genes that exhibit spatial expression patterns within small ROIs but are not marker genes of the ROIs. These genes, referred to as *spatial-domain-specific SVGs*, cannot be detected by methods that identify spatial-domain-marker SVGs and can also be missed by methods that detect overall SVGs. Although no existing methods are specifically designed for detecting these spatial-domain-specific SVGs, methods for detecting overall SVGs can presumably be applied to specific spatial domains to discover these genes. Third, cell-type-specific SVGs might also be easily missed by methods that detect overall SVGs if the cell types of interest have small proportions. To address this, methods for detecting cell-type-specific SVGs have been developed, including CTSV [54], C-SIDE [56], and spVC [57]. These methods rely on regression models, whose goodness-of-fit to SRT data remains to be explored. Ensuring a good fit is essential to avoid spurious discoveries. Fourth, some genes may exhibit sharp expression changes at tissue layer boundaries, which are too local to be detected by methods looking for overall SVGs. Belayer [72] aims to detect such genes by examining gene expression change rates (gradients) in the 2D space. As a future direction, adding the accompanying H&E image can help refine tissue boundaries, ensuring that the identified genes are interpretable. Moreover, if users have prior knowledge on some interesting genes that should be detected as SVGs, how to incorporate this knowledge into SVG detection to improve the specificity remains an open question.

The scalability of an SVG detection method is determined by the computational time of two

steps: calculating a summary statistic for each gene and converting the summary statistic to a p-value based on a null distribution. The second step is only included in methods that provide statistical significance for the detected SVGs in a frequentist manner. For the first step, computational time is measured in terms of n , the number of spatial spots. For example, fitting a Gaussian process takes $O(n^3)$ time in SpatialDE [20] and SPARK [25], but this time is reduced to $O(n)$ by using the nearest-neighbor Gaussian process approximation in nnSVG [21]. By changing the modeling framework from a Gaussian process to a Pearson correlation between two similarity matrices, SPARK-X [28] also achieves a fast computational time of $O(n)$. For the second step, computational time is fast if the summary statistic has a closed-form null distribution, as is the case for most methods using conventional statistics under regression frameworks. However, for methods using unconventional statistics, the null distribution is usually derived by permutation, which is computationally intensive. To improve the scalability of a method, considerations can be put into expediting both steps, for example, by using approximation algorithms to speed up the first step and reducing the number of permutations in the second step [73, 74].

8.2 Future direction 1: Accommodating SRT technological differences

Two key differences exist among SRT technologies. However, most of current SVG detection methods do not consider these technological differences when pre-processing and modeling SRT data. Below, we introduce the differences and their potential effects on SVG detection.

1. **Spatial resolution.** Imaging-based SRT measures per transcript's spatial localization at a single-cell or subcellular resolution, whereas sequencing-based SRT captures data at a multicellular level with relatively coarse resolution. In imaging-based SRT data, detected SVGs might result from the irregular distribution of cell types, such as cancer cells spreading across tumor tissue or mixed cell types at the boundaries of tissue layers. In contrast, the coarse resolution of sequencing-based SRT likely results in smaller variance of gene expression levels across spatial spots compared to imaging-based SRT data. Consequently, the spatial resolution differences between the two types of SRT technologies necessitate different interpretations for the detected SVGs. However, most existing SVG detection methods do not distinguish between the SRT technologies but use the same approach to identify SVGs, indicating a need for improvement.

2. **Positional randomness of spatial spots.** Different SRT technologies use various strategies to record the positions of spatial spots, resulting in differences in positional randomness. For instance, technologies like Spatial Transcriptomics and 10x Visium capture transcripts in predefined rectilinear or hexagonal grids on micro-slides, leading to structured spatial spots that lack positional randomness. In contrast, technologies like Slide-seq, MERFISH, and SeqFISH capture transcripts wherever they are located, without using predefined grids, leading to unstructured spatial spots with positional randomness. This difference in spatial positional randomness necessitates different modeling strategies for spatial variance. For example, sepal [32] designs

distinct spatial modeling frameworks—rectilinear, hexagonal, and unstructured spots—for Spatial Transcriptomics, 10x Visium, and Slide-seq, respectively. MERINGUE [75] and several other graph-based methods use Delaunay triangulation to account for the nonuniform density of unstructured spots. BOOST-HMI [39] uses the mark interaction model, an extension of the Ising model used in BOOST-MI, to address the irregular distribution of spatial spots for imaging-based SRT data. However, the majority of SVG detection methods have not considered the positional randomness differences among SRT technologies, potentially leading to biased detection of SVGs.

8.3 Fugure direction 2: Enhancing statistical rigor and method validation

Similar to single-cell RNA-seq data analysis [76–78], SRT data analysis faces the “double-dipping” challenge: the same data are analyzed more than once, and the final statistical tests rely on variables inferred from the same data in previous steps, leading to a “confirmation bias”. This issue is prominent in spatial-domain-marker SVG detection, where the genes involved in identifying spatial domains would inherently be identified as spatial-domain markers in a subsequent step, even if they do not exhibit significant expression changes between spatial domains. Therefore, strategies are needed to remove false-positive discoveries resulting from double-dipping, such as those employed in ClusterDE [78].

Moreover, as many SVG detection methods use complex algorithms with implicit assumptions, interpretable ways for sanity checks on the detected SVGs are essential. For example, using *in silico* negative control SRT data can help users test SVG detection methods and identify spurious discoveries. Additionally, fast visualization tools will assist users in interpreting the top detected SVGs, providing a clearer understanding of the results and enhancing the reliability of the findings.

No method can be optimal in every aspect, making method choice for users’ goals crucial. Users should select methods that capture the spatial patterns of interest, ensuring the method’s strengths align with their research needs. Consequently, the diversity of methods is indispensable to cater to various user needs, and method validation and benchmarking are necessary for users to choose the appropriate methods. However, benchmarking is challenging due to the lack of well-annotated datasets with SVG ground truths. As a result, methods often justify their effectiveness indirectly, which may or may not reflect the biological questions users seek answers for. Early methods like SpatialDE and Trendsceek validate their detected SVGs by visual inspection. Another prevalent strategy is to use synthetic datasets with artificial spatial patterns, such as hotspots, streaks, and rings (Fig. 5a), to evaluate methods’ detection power. However, these artificial patterns are oversimplified and might not be biologically relevant (Fig. 5b). Hence, benchmarking needs well-annotated SRT datasets from diverse tissues (e.g., structured tissues like the brain and unstructured tissues like tumors) or realistic SRT data simulators [79, 80], not only for comprehensive method validation but also for the potential development of supervised methods. We curated the SRT datasets used by the existing SVG detection methods in Supplementary File.

9 Conclusion

In this article, we review 31 peer-reviewed SVG detection methods for SRT data, focusing on the SVG definitions, detection methodologies, and biological implications. To avoid the ambiguity of terminology, we classify the 31 methods into three main categories based on the SVGs they detect: overall SVGs, cell-type-specific SVGs, and spatial-domain-marker SVGs (Fig. 2–4; Table 1). We summarize these methods in Tables 2–3, including input data, modeling framework, and availability of statistical significance. Next, we introduce the downstream applications of SVGs, including identifying spatial domains with marker genes and spatial patterns of cell types or states. Furthermore, from a statistical perspective, we divide the frequentist hypothesis tests used in 21 methods into three types: dependence tests, regression fixed-effect tests, and regression random-effect tests (Table 1). We summarize how the three types of hypothesis tests are used to detect SVGs and discuss how they differ from each other regarding the generality and specificity for SVG detection. Finally, we discuss the comparative advantages of existing SVG detection methods and offer insights into the future directions for improvement.

Competing interests

The authors declare no competing interests.

Acknowledgements

The authors appreciate the comments and feedback from the members of the Junction of Statistics and Biology at UCLA (<http://jsb.ucla.edu>).

Funding

This work was supported by the following grants: National Science Foundation DBI-1846216 and DMS-2113754, NIH/NIGMS R01GM120507 and R35GM140888, Johnson & Johnson WiSTEM2D Award, Sloan Research Fellowship, UCLA David Geffen School of Medicine W.M. Keck Foundation Junior Faculty Award, and Chan-Zuckerberg Initiative Single-Cell Biology Data Insights [Silicon Valley Community Foundation Grant Number: 2022-249355] (to J.J.L.). J.J.L. was a fellow at the Radcliffe Institute for Advanced Study at Harvard University in 2022–2023 while she was writing this paper.

Figures

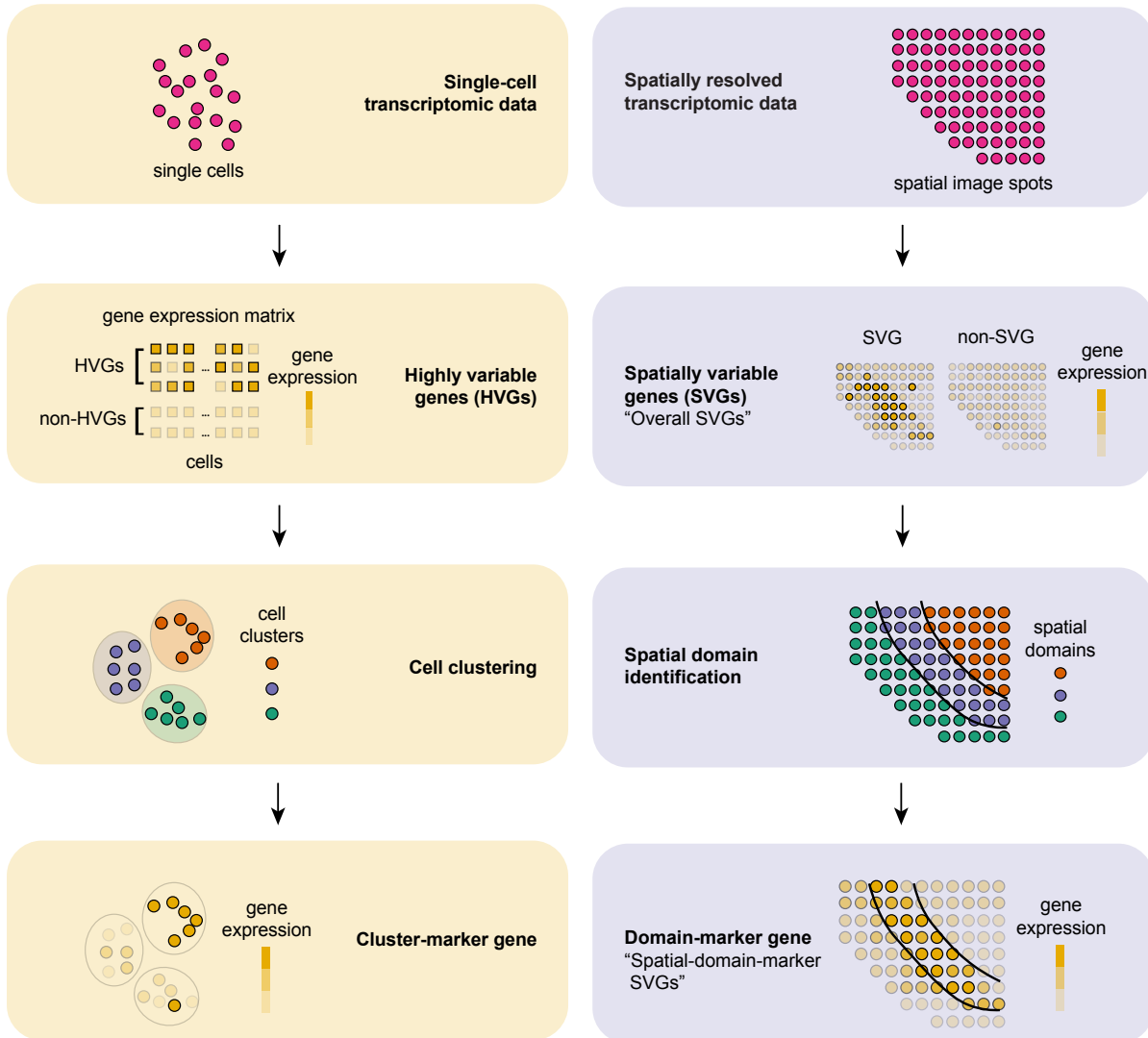


Figure 1: General analysis workflows of single-cell transcriptomic data and spatially resolved transcriptomic (SRT) data. The left column shows a general analysis workflow for single-cell transcriptomic data with steps including highly variable gene (HVG) detection, cell clustering, and cluster-marker gene identification. The right column illustrates the workflow for analyzing SRT data with steps including spatially variable gene (SVG) detection, spatial domain identification, and domain-marker gene identification.

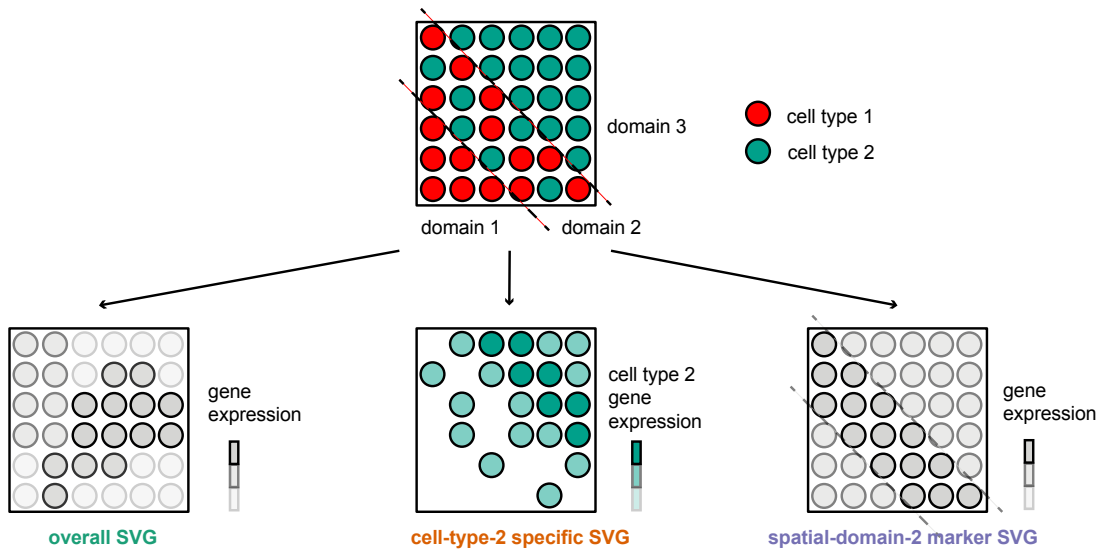


Figure 2: Conceptual visualization of three SVG categories: overall SVGs, cell-type-specific SVGs, and spatial-domain-marker SVGs. The top row shows a tissue slice with two cell types and three spatial domains. From left to right, exemplar genes with colors representing the expression levels are shown for an overall SVG, a cell-type-specific SVG, and a spatial-domain-marker SVG, respectively.

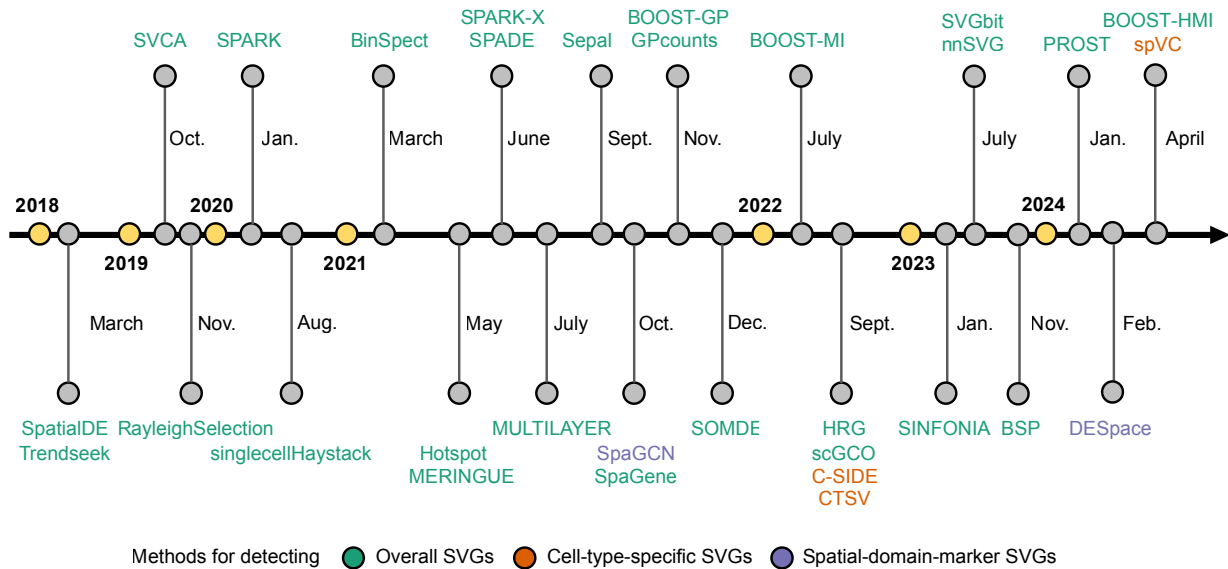


Figure 3: Publication timeline of 31 SVG detection methods. Colors represent three SVG categories: overall SVGs (green), cell-type-specific SVGs (red), and spatial-domain-marker SVGs (purple).

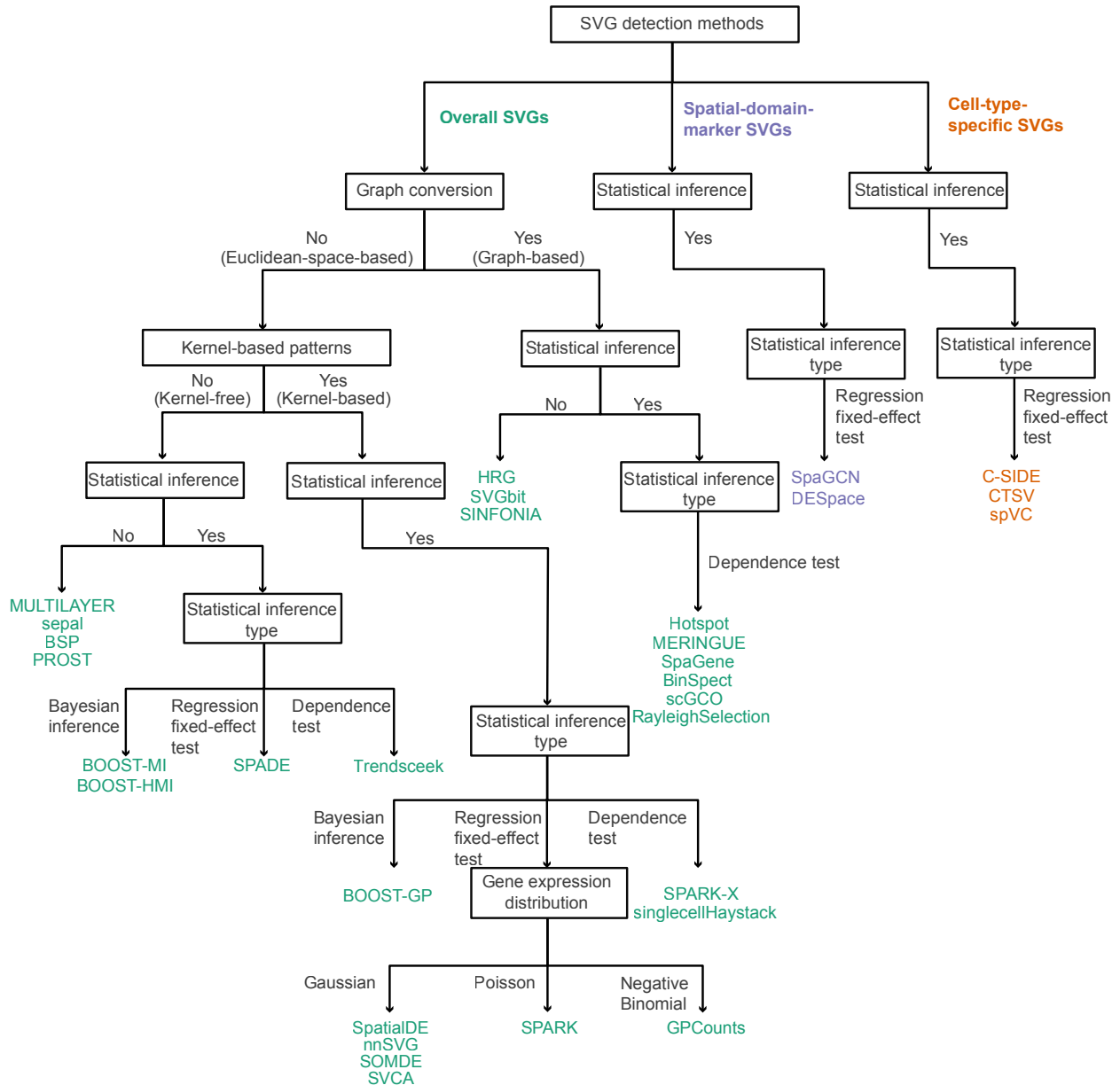


Figure 4: A hierarchical summary of 31 SVG detection methods. The hierarchical summary considers the methodological characteristics, including graph conversion, kernel-based patterns, availability of statistical inference, statistical inference types, and gene expression distributions. Colors represent three SVG categories: overall SVGs (green), cell-type-specific SVGs (red), and spatial-domain-marker SVGs (purple).

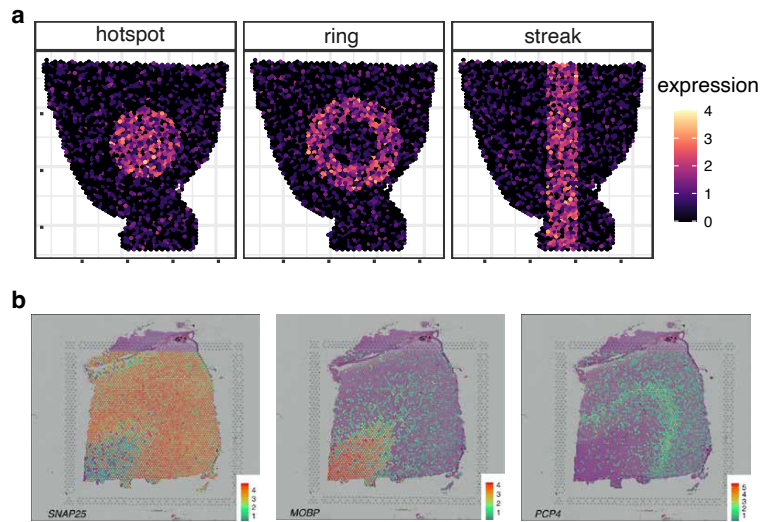


Figure 5: Synthetic spatial patterns oversimplify the spatial patterns observed in real SRT data. **a**, Representative spatial patterns used in synthetic SRT data for evaluating SVG detection methods such as Trendsceek [30], SpatialIDE [20], and others. **b**, Spatial patterns shown in the 10x Visium dataset [67] profiling a dorsal lateral prefrontal cortex sample. The color indicates the log transformed expression for genes *SNAP25*, *MOBP*, and *PCP4*.

Tables

Table 1: Classification of 31 SVG detection methods along with statistical inference types

Inference types		Categories	Overall SVGs	Cell-type-specific SVGs	Spatial-domain-marker SVGs
Frequentist inference	Dependence tests	SPARK-X singlecellHaystack Trendsceek Hotspot MERINGUE SpaGene BinSpect scGCO RayleighSelection			
	Regression fixed-effect tests	SPADE	CTSV C-SIDE spVC	SpaGCN DESpace	
	Regression random-effect tests	SpatialDE nnSVG SOMDE SVCA SPARK GPcounts			
Bayesian inference			BOOST-GP BOOST-MI BOOST-HMI		
No statistical inference			MULTILAYER sepal BSP ¹ PROST ² HRG SVGbit SINFONIA		

¹ Although BSP attempts to perform frequentist inference by defining a null distribution for its test statistic, the null distribution is improperly defined as a distribution fitted to the test statistic values of all genes, implying that all genes are non-SVGs. Hence, we do not label BSP as a method with statistical inference in the table.

² PROST performs frequentist statistical tests for Moran's I, instead of the PROST index it uses to rank genes as SVGs.

Table 2: Methodological traits of 31 SVG detection methods.

Method	Category	Statistical framework			Count modeling	Statistical inference (frequentist or Bayesian hypothesis tests)
		Graph-based	Euclidean-space-based			
			Kernel-based	Kernel-free		
SpatialDE	Overall SVG		✓			✓ (Frequentist)
nnSVG	Overall SVG		✓			✓ (Frequentist)
SOMDE	Overall SVG		✓			✓ (Frequentist)
SVCA	Overall SVG		✓			✓ (Frequentist)
SPARK	Overall SVG		✓		✓	✓ (Frequentist)
GPcounts	Overall SVG		✓		✓	✓ (Frequentist)
BOOST-GP	Overall SVG		✓		✓	✓ (Bayesian)
SPARK-X	Overall SVG		✓			✓ (Frequentist)
singlecellHaystack	Overall SVG		✓			✓ (Frequentist)
Trendsceek	Overall SVG			✓		✓ (Frequentist)
MULTILAYER	Overall SVG			✓		
sepal	Overall SVG			✓		
BSP	Overall SVG			✓		
PROST	Overall SVG			✓		
SPADE	Overall SVG			✓		✓ (Frequentist)
BOOST-MI	Overall SVG			✓		✓ (Bayesian)
BOOST-HMI	Overall SVG			✓	✓	✓ (Bayesian)
Hotspot	Overall SVG	✓				✓ (Frequentist)
HRG	Overall SVG	✓				
SVGbit	Overall SVG	✓				
SINFONIA	Overall SVG	✓				
MERINGUE	Overall SVG	✓				✓ (Frequentist)
SpaGene	Overall SVG	✓				✓ (Frequentist)
BinSpect	Overall SVG	✓				✓ (Frequentist)
scGCO	Overall SVG	✓				✓ (Frequentist)
RayleighSelection	Overall SVG	✓				✓ (Frequentist)
CTSV	Cell-type-specific SVG			✓	✓	✓ (Frequentist)
C-SIDE	Cell-type-specific SVG			✓	✓	✓ (Frequentist)
spVC	Cell-type-specific SVG			✓	✓	✓ (Frequentist)
SpaGCN	Spatial-domain-marker SVG			✓		✓ (Frequentist)
DESpace	Spatial-domain-marker SVG			✓	✓	✓ (Frequentist)

Table 3: Characteristics of 21 frequentist-hypothesis-tests-based SVG detection methods.^{1,2}

Method	Gene expression modeling	Spatial location modeling	Hypothesis test type	Null hypothesis	Test statistics	Null distribution
SpatialDE	Gaussian distribution	Gaussian process	Regression random-effect test	Spatial covariance has no contribution to gene expression variance	LRT statistic	Chi-square
nnSVG						
SOMDE						
SVCA						
SPARK	Poisson / Gaussian distribution					
GPcounts	Negative binomial distribution					
SPARK-X	Spot-spot similarity		Dependence test	Spatial location and gene expression are independent	Pearson correlation of spot-spot location similarity matrix and gene expression similarity matrix	Chi-square
singlecellHaystack	Dichotomization	Nonparametric distribution			KL divergence	Permutation
Trendsceek	Marked point process				Mark-segregation summary statistics	
SPADE	Gaussian distribution	Feature extracted by CNN	Regression fixed-effect test	Spatial location has no effect on gene expression	t-statistic	Student's t-distribution
Hotspot	Autocorrelation statistic		Dependence test	A gene's expression counts at spots independently follow negative binomial or Bernoulli distribution	z-score	Standard normal
MERINGUE	Moran's I			A gene's expression levels at spots have no spatial autocorrelations	z-score	
SpaGene	Dichotomization	Node degree distribution in a KNN graph		Spatial location and gene expression are independent	Earth mover's distance	Permutation
BinSpect		Edges in a graph			Fisher's exact test statistic	Hypergeometric distribution
scGCO	Gaussian mixture model (GMM) & Hidden Markov random field (HMRF)	Hidden Markov random field		Spatial location and gene expression are independent	Proportion of spots with a particular level (from GMM) within a spatial segment (from HMRF)	Homogeneous Poisson process
RayleighSelection	Combinatorial Laplacian score for a simplicial complex				Combinatorial Laplacian score	Permutation

¹ The 21 SVG detection methods using frequentist statistical hypothesis tests (Table 2) are included in this table.

² The table is continued on the next page.

Table 3: Characteristics of 21 frequentist-hypothesis-tests-based SVG detection methods. (continued)

Method	Gene expression modeling	Spatial location modeling	Hypothesis test type	Null hypothesis	Test statistics	Null distribution
CTSV	Zero-inflated negative binomial	Fixed-effect covariate (spatial location) in a generalized additive model	Regression fixed-effect test	Spatial location has no effect on cell-type-specific gene expression	Wald statistic	Chi-square
C-SIDE	Poisson				z-score	Standard normal
spVC	Poisson				LRT statistic and Wald statistic	Chi-square
SpaGCN	Graph convolutional network			No differential gene expression between spatial domains	Wilcoxon rank sum	Standard normal
DESpace	Negative binomial	Fixed-effect covariate (spatial domain) in a generalized linear model			LRT statistic	Chi-square

References

- [1] SK Longo, MG Guo, AL Ji, and PA Khavari. Integrating single-cell and spatial transcriptomics to elucidate intercellular tissue dynamics. *Nat Rev Genet*, 22:627–644, Oct 2021.
- [2] Vivien Marx. Method of the year: spatially resolved transcriptomics. *Nature methods*, 18(1): 9–14, 2021.
- [3] R Ke, M Mignardi, A Pacureanu, J Svedlund, J Botling, C Wählby, and M Nilsson. In situ sequencing for RNA analysis in preserved tissue and cells. *Nat Methods*, 10:857–60, Sep 2013.
- [4] Eric Lubeck, Ahmet F Coskun, Timur Zhiyentayev, Mubhij Ahmad, and Long Cai. Single-cell in situ RNA profiling by sequential hybridization. *Nature methods*, 11(4):360–361, 2014.
- [5] Sheel Shah, Eric Lubeck, Wen Zhou, and Long Cai. In situ transcription profiling of single cells reveals spatial organization of cells in the mouse hippocampus. *Neuron*, 92(2):342–357, 2016.
- [6] Chee-Huat Linus Eng, Michael Lawson, Qian Zhu, Ruben Dries, Noushin Koulana, Yodai Takei, Jina Yun, Christopher Cronin, Christoph Karp, Guo-Cheng Yuan, et al. Transcriptome-scale super-resolved imaging in tissues by RNA seqFISH+. *Nature*, 568(7751):235–239, 2019.
- [7] KH Chen, AN Boettiger, JR Moffitt, S Wang, and X Zhuang. Spatially resolved, highly multiplexed RNA profiling in single cells. *Science* 348: aaa6090, 2015.
- [8] Xiao Wang, William E Allen, Matthew A Wright, Emily L Sylwestrak, Nikolay Samusik, Sam Vesuna, Kathryn Evans, Cindy Liu, Charu Ramakrishnan, Jia Liu, et al. Three-dimensional intact-tissue sequencing of single-cell transcriptional states. *Science*, 361(6400):eaat5691, 2018.
- [9] Shahar Alon, Daniel R Goodwin, Anubhav Sinha, Asmamaw T Wassie, Fei Chen, Evan R Daugharthy, Yosuke Bando, Atsushi Kajita, Andrew G Xue, Karl Marrett, et al. Expansion sequencing: Spatially precise in situ transcriptomics in intact biological systems. *Science*, 371(6528):eaax2656, 2021.
- [10] Amanda Janesick, Robert Shelansky, Andrew D Gottscho, Florian Wagner, Stephen R Williams, Morgane Rouault, Ghezal Beliakoff, Carolyn A Morrison, Michelli F Oliveira, Jordan T Sicherman, et al. High resolution mapping of the tumor microenvironment using integrated single-cell, spatial and in situ analysis. *Nature Communications*, 14(1):8353, 2023.
- [11] 10xGenomics. Inside visium spatial capture technology, 2019. https://pages.10xgenomics.com/rs/446-PB0-704/images/10x_BR060_Inside_Visium_Spatial_Technology.pdf.

- [12] Samuel G Rodriques, Robert R Stickels, Aleksandrina Goeva, Carly A Martin, Evan Murray, Charles R Vanderburg, Joshua Welch, Linlin M Chen, Fei Chen, and Evan Z Macosko. Slide-seq: A scalable technology for measuring genome-wide expression at high spatial resolution. *Science*, 363(6434):1463–1467, 2019.
- [13] Daniel R Zollinger, Stan E Lingle, Kristina Sorg, Joseph M Beechem, and Christopher R Merritt. Geomx™ rna assay: high multiplex, digital, spatial analysis of rna in ffpe tissue. In *In Situ Hybridization Protocols*, pages 331–345. Springer, 2020.
- [14] Ao Chen, Sha Liao, Mengnan Cheng, Kailong Ma, Liang Wu, Yiwei Lai, Xiaojie Qiu, Jin Yang, Jiangshan Xu, Shijie Hao, et al. Spatiotemporal transcriptomic atlas of mouse organogenesis using dna nanoball-patterned arrays. *Cell*, 185(10):1777–1792, 2022.
- [15] Chun-Seok Cho, Jingyue Xi, Yichen Si, Sung-Rye Park, Jer-En Hsu, Myungjin Kim, Goo Jun, Hyun Min Kang, and Jun Hee Lee. Microscopic examination of spatial transcriptome using seq-scope. *Cell*, 184(13):3559–3572, 2021.
- [16] Sikta Das Adhikari, Jiaxin Yang, Jianrong Wang, and Yuehua Cui. Recent advances in spatially variable gene detection in spatial transcriptomics. *Computational and Structural Biotechnology Journal*, 2024.
- [17] Zhijian Li, Zain M Patel, Dongyuan Song, Guanao Yan, Jingyi Jessica Li, and Luca Pinello. Benchmarking computational methods to identify spatially variable genes and peaks. *Biorxiv*, pages 2023–12, 2023.
- [18] Carissa Chen, Hani Jieun Kim, and Pengyi Yang. Evaluating spatially variable gene detection methods for spatial transcriptomics data. *Genome Biology*, 25(1):18, 2024.
- [19] Natalie Charitakis, Agus Salim, Adam T Piers, Kevin I Watt, Enzo R Porrello, David A Elliott, and Mirana Ramialison. Disparities in spatially variable gene calling highlight the need for benchmarking spatial transcriptomics methods. *Genome Biology*, 24(1):209, 2023.
- [20] Valentine Svensson, Sarah A Teichmann, and Oliver Stegle. SpatialDE: identification of spatially variable genes. *Nature methods*, 15(5):343–346, 2018.
- [21] Lukas M Weber, Arkajyoti Saha, Abhirup Datta, Kasper D Hansen, and Stephanie C Hicks. *Nature Communications*, 14(1):4059, 2023.
- [22] Abhirup Datta, Sudipto Banerjee, Andrew O Finley, and Alan E Gelfand. Hierarchical nearest-neighbor gaussian process models for large geostatistical datasets. *Journal of the American Statistical Association*, 111(514):800–812, 2016.
- [23] Minsheng Hao, Kui Hua, and Xuegong Zhang. SOMDE: a scalable method for identifying spatially variable genes with self-organizing map. *Bioinformatics*, 37(23):4392–4398, 2021.

- [24] Damien Arno, Denis Schapiro, Bernd Bodenmiller, Julio Saez-Rodriguez, and Oliver Stegle. Modeling cell-cell interactions from spatial molecular data with spatial variance component analysis. *Cell reports*, 29(1):202–211, 2019.
- [25] Shiquan Sun, Jiaqiang Zhu, and Xiang Zhou. Statistical analysis of spatial expression patterns for spatially resolved transcriptomic studies. *Nature methods*, 17(2):193–200, 2020.
- [26] Nuha BinTayyash, Sokratia Georgaka, S T John, Sumon Ahmed, Alexis Boukouvalas, James Hensman, and Magnus Rattray. Non-parametric modelling of temporal and spatial counts data from RNA-seq experiments. *Bioinformatics*, 37(21):3788–3795, 2021.
- [27] Qiwei Li, Minzhe Zhang, Yang Xie, and Guanghua Xiao. Bayesian modeling of spatial molecular profiling data via Gaussian process. *Bioinformatics*, 37(22):4129–4136, 2021.
- [28] Jiaqiang Zhu, Shiquan Sun, and Xiang Zhou. Spark-x: non-parametric modeling enables scalable and robust detection of spatial expression patterns for large spatial transcriptomic studies. *Genome biology*, 22(1):1–25, 2021.
- [29] Alexis Vandenberg and Diego Diez. A clustering-independent method for finding differentially expressed genes in single-cell transcriptome data. *Nature communications*, 11(1):1–10, 2020.
- [30] Daniel Edsgård, Per Johnsson, and Rickard Sandberg. Identification of spatial expression trends in single-cell gene expression data. *Nature methods*, 15(5):339–342, 2018.
- [31] Julien Moehlin, Bastien Mollet, Bruno Maria Colombo, and Marco Antonio Mendoza-Parra. Inferring biologically relevant molecular tissue substructures by agglomerative clustering of digitized spatial transcriptomes with multilayer. *Cell Systems*, 12(7):694–705, 2021.
- [32] Alma Andersson and Joakim Lundeberg. sepal: identifying transcript profiles with spatial patterns by diffusion-based modeling. *Bioinformatics*, 37(17):2644–2650, 2021.
- [33] Leonid Vital'evich Kantorovich. Approximate methods of higher analysis. *Interscience*, 1958.
- [34] Juexin Wang, Jinpu Li, Skyler T Kramer, Li Su, Yuzhou Chang, Chunhui Xu, Michael T Eadon, Krzysztof Kiryluk, Qin Ma, and Dong Xu. Dimension-agnostic and granularity-based spatially variable gene identification using bsp. *Nature Communications*, 14(1):7367, 2023.
- [35] Yuchen Liang, Guowei Shi, Runlin Cai, Yuchen Yuan, Ziyang Xie, Long Yu, Yingjian Huang, Qian Shi, Lizhe Wang, Jun Li, et al. Prost: quantitative identification of spatially variable genes and domain detection in spatial transcriptomics. *Nature Communications*, 15(1):600, 2024.
- [36] Patrick AP Moran. Notes on continuous stochastic phenomena. *Biometrika*, 37(1/2):17–23, 1950.

- [37] Sungwoo Bae, Hongyoon Choi, and Dong Soo Lee. Discovery of molecular features underlying the morphological landscape by integrating spatial transcriptomic data with deep features of tissue images. *Nucleic acids research*, 49(10):e55–e55, 2021.
- [38] Xi Jiang, Guanghua Xiao, and Qiwei Li. A bayesian modified ising model for identifying spatially variable genes from spatial transcriptomics data. *Statistics in Medicine*, 41(23):4647–4665, 2022.
- [39] Jie Yang, Xi Jiang, Kevin Wang Jin, Sunyoung Shin, and Qiwei Li. Bayesian hidden mark interaction model for detecting spatially variable genes in imaging-based spatially resolved transcriptomics data. *Frontiers in Genetics*, 15:1356709, 2024.
- [40] David DeTomaso and Nir Yosef. Hotspot identifies informative gene modules across modalities of single-cell genomics. *Cell systems*, 12(5):446–456, 2021.
- [41] Yanhong Wu, Qifan Hu, Shicheng Wang, Changyi Liu, Yiran Shan, Wenbo Guo, Rui Jiang, Xiaowo Wang, and Jin Gu. Highly regional genes: graph-based gene selection for single-cell rna-seq data. *Journal of Genetics and Genomics*, 2022.
- [42] Yingzhou Hong, Kai Song, Zongbo Zhang, Yuxia Deng, Xue Zhang, Jinqian Zhao, Jun Jiang, Qing Zhang, Chunming Guo, and Cheng Peng. The spatiotemporal dynamics of spatially variable genes in developing mouse brain revealed by a novel computational scheme. *Cell Death Discovery*, 9(1):264, 2023.
- [43] Rui Jiang, Zhen Li, Yuhang Jia, Siyu Li, and Shengquan Chen. Sinfonia: Scalable identification of spatially variable genes for deciphering spatial domains. *Cells*, 12(4):604, 2023.
- [44] Robert C Geary. The contiguity ratio and statistical mapping. *The incorporated statistician*, 5(3):115–146, 1954.
- [45] Brendan F Miller, Dhananjay Bambah-Mukku, Catherine Dulac, Xiaowei Zhuang, and Jean Fan. Characterizing spatial gene expression heterogeneity in spatially resolved single-cell transcriptomic data with nonuniform cellular densities. *Genome research*, 31(10):1843–1855, 2021.
- [46] Franco P Preparata and Michael I Shamos. *Computational geometry: an introduction*. Springer Science & Business Media, 2012.
- [47] Qi Liu, Chih-Yuan Hsu, and Yu Shyr. Scalable and model-free detection of spatial patterns and colocalization. *Genome Research*, 32(9):1736–1745, 2022.
- [48] Ruben Dries, Qian Zhu, Rui Dong, Chee-Huat Linus Eng, Huipeng Li, Kan Liu, Yuntian Fu, Tianxiao Zhao, Arpan Sarkar, Feng Bao, et al. Giotto: a toolbox for integrative analysis and visualization of spatial expression data. *Genome biology*, 22(1):1–31, 2021.

- [49] Yuhan Hao, Stephanie Hao, Erica Andersen-Nissen, William M. Mauck III, Shiwei Zheng, Andrew Butler, Maddie J. Lee, Aaron J. Wilk, Charlotte Darby, Michael Zagar, Paul Hoffman, Marlon Stoeckius, Efthymia Papalexi, Eleni P. Mimitou, Jaison Jain, Avi Srivastava, Tim Stuart, Lamar B. Fleming, Bertrand Yeung, Angela J. Rogers, Juliana M. McElrath, Catherine A. Blish, Raphael Gottardo, Peter Smibert, and Rahul Satija. Integrated analysis of multimodal single-cell data. *Cell*, 2021. doi: 10.1016/j.cell.2021.04.048. URL <https://doi.org/10.1016/j.cell.2021.04.048>.
- [50] Giovanni Palla, Hannah Spitzer, Michal Klein, David Fischer, Anna Christina Schaar, Louis Benedikt Kuemmerle, Sergei Rybakov, Ignacio L Ibarra, Olle Holmberg, Isaac Virshup, et al. Squidpy: a scalable framework for spatial omics analysis. *Nature methods*, 19(2): 171–178, 2022.
- [51] Ke Zhang, Wanwan Feng, and Peng Wang. Identification of spatially variable genes with graph cuts. *Nature Communications*, 13(1):1–15, 2022.
- [52] Kiya W Govek, Venkata S Yamajala, and Pablo G Camara. Clustering-independent analysis of genomic data using spectral simplicial theory. *PLoS computational biology*, 15(11): e1007509, 2019.
- [53] Danijela Horak and Jürgen Jost. Spectra of combinatorial laplace operators on simplicial complexes. *Advances in Mathematics*, 244:303–336, 2013.
- [54] Jinge Yu and Xiangyu Luo. Identification of cell-type-specific spatially variable genes accounting for excess zeros. *Bioinformatics*, 38(17):4135–4144, 2022.
- [55] Dylan M Cable, Evan Murray, Luli S Zou, Aleksandrina Goeva, Evan Z Macosko, Fei Chen, and Rafael A Irizarry. Robust decomposition of cell type mixtures in spatial transcriptomics. *Nature Biotechnology*, 40(4):517–526, 2022.
- [56] Dylan M Cable, Evan Murray, Vignesh Shanmugam, Simon Zhang, Luli S Zou, Michael Diao, Haiqi Chen, Evan Z Macosko, Rafael A Irizarry, and Fei Chen. Cell type-specific inference of differential expression in spatial transcriptomics. *Nature methods*, 19(9):1076–1087, 2022.
- [57] Shan Yu and Wei Vivian Li. spvc for the detection and interpretation of spatial gene expression variation. *Genome Biology*, 25(1):103, 2024.
- [58] Marc Elosua-Bayes, Paula Nieto, Elisabetta Mereu, Ivo Gut, and Holger Heyn. Spotlight: seeded nmf regression to deconvolute spatial transcriptomics spots with single-cell transcriptomes. *Nucleic acids research*, 49(9):e50–e50, 2021.
- [59] Jian Hu, Xiangjie Li, Kyle Coleman, Amelia Schroeder, Nan Ma, David J Irwin, Edward B Lee, Russell T Shinohara, and Mingyao Li. Spagcn: Integrating gene expression, spatial location and histology to identify spatial domains and spatially variable genes by graph convolutional network. *Nature methods*, 18(11):1342–1351, 2021.

- [60] Peiyong Cai, Mark D Robinson, and Simone Tiberi. Despace: spatially variable gene detection via differential expression testing of spatial clusters. *Bioinformatics*, 40(2):btac027, 2024.
- [61] Edward Zhao, Matthew R Stone, Xing Ren, Jamie Guenthoer, Kimberly S Smythe, Thomas Pulliam, Stephen R Williams, Cedric R Uyttingco, Sarah EB Taylor, Paul Nghiem, et al. Spatial transcriptomics at subspot resolution with bayesspace. *Nature biotechnology*, 39(11):1375–1384, 2021.
- [62] Duy Pham, Xiao Tan, Brad Balderson, Jun Xu, Laura F Grice, Sohye Yoon, Emily F Willis, Minh Tran, Pui Yeng Lam, Arti Raghobar, et al. Robust mapping of spatiotemporal trajectories and cell–cell interactions in healthy and diseased tissues. *Nature communications*, 14(1):7739, 2023.
- [63] Ke Zhang, Wanwan Feng, and Peng Wang. Identification of spatially variable genes with graph cuts. *Nature Communications*, 13(1):1–15, 2022.
- [64] Patrik L Ståhl, Fredrik Salmén, Sanja Vickovic, Anna Lundmark, José Fernández Navarro, Jens Magnusson, Stefania Giacomello, Michaela Asp, Jakub O Westholm, Mikael Huss, et al. Visualization and analysis of gene expression in tissue sections by spatial transcriptomics. *Science*, 353(6294):78–82, 2016.
- [65] Robert R Stickels, Evan Murray, Pawan Kumar, Jilong Li, Jamie L Marshall, Daniela J Di Bella, Paola Arlotta, Evan Z Macosko, and Fei Chen. Highly sensitive spatial transcriptomics at near-cellular resolution with slide-seq2. *Nature biotechnology*, 39(3):313–319, 2021.
- [66] Wei Guo, Bolun Zhou, Zhenlin Yang, Xiang Liu, Qilin Huai, Lei Guo, Xuemin Xue, Fengwei Tan, Yin Li, Qi Xue, et al. Integrating microarray-based spatial transcriptomics and single-cell rna-sequencing reveals tissue architecture in esophageal squamous cell carcinoma. *EBioMedicine*, 84, 2022.
- [67] Kristen R Maynard, Leonardo Collado-Torres, Lukas M Weber, Cedric Uyttingco, Brianna K Barry, Stephen R Williams, Joseph L Catallini, Matthew N Tran, Zachary Besich, Madhavi Tippani, et al. Transcriptome-scale spatial gene expression in the human dorsolateral prefrontal cortex. *Nature neuroscience*, 24(3):425–436, 2021.
- [68] Susan M Sunkin, Lydia Ng, Chris Lau, Tim Dolbeare, Terri L Gilbert, Carol L Thompson, Michael Hawrylycz, and Chinh Dang. Allen brain atlas: an integrated spatio-temporal portal for exploring the central nervous system. *Nucleic acids research*, 41(D1):D996–D1008, 2012.
- [69] Jingyi Jessica Li, Heather J Zhou, Peter J Bickel, and Xin Tong. Dissecting gene expression heterogeneity: generalized pearson correlation squares and the k-lines clustering algorithm. *Journal of the American Statistical Association*, (just-accepted):1–22, 2024.

- [70] Yumei Li, Xinzhou Ge, Fanglue Peng, Wei Li, and Jingyi Jessica Li. Exaggerated false positives by popular differential expression methods when analyzing human population samples. *Genome biology*, 23(1):79, 2022.
- [71] Matthew E Ritchie, Belinda Phipson, DI Wu, Yifang Hu, Charity W Law, Wei Shi, and Gordon K Smyth. limma powers differential expression analyses for rna-sequencing and microarray studies. *Nucleic acids research*, 43(7):e47–e47, 2015.
- [72] Cong Ma, Uthsav Chitra, Shirley Zhang, and Benjamin J Raphael. Belayr: Modeling discrete and continuous spatial variation in gene expression from spatially resolved transcriptomics. *Cell systems*, 13(10):786–797, 2022.
- [73] Xinzhou Ge, Yiling Elaine Chen, Dongyuan Song, MeiLu McDermott, Kyla Woysner, Antigoni Manousopoulou, Ning Wang, Wei Li, Leo D Wang, and Jingyi Jessica Li. Clipper: p-value-free fdr control on high-throughput data from two conditions. *Genome biology*, 22: 1–29, 2021.
- [74] Dongyuan Song and Jingyi Jessica Li. Pseudotime: inference of differential gene expression along cell pseudotime with well-calibrated p-values from single-cell rna sequencing data. *Genome biology*, 22(1):124, 2021.
- [75] Brendan F Miller, Dhananjay Bambah-Mukku, Catherine Dulac, Xiaowei Zhuang, and Jean Fan. Characterizing spatial gene expression heterogeneity in spatially resolved single-cell transcriptomic data with nonuniform cellular densities. *Genome research*, 31(10):1843–1855, 2021.
- [76] Jesse M Zhang, Govinda M Kamath, and N Tse David. Valid post-clustering differential analysis for single-cell rna-seq. *Cell systems*, 9(4):383–392, 2019.
- [77] Anna Neufeld, Lucy L Gao, Joshua Popp, Alexis Battle, and Daniela Witten. Inference after latent variable estimation for single-cell rna sequencing data. *Biostatistics*, 25(1):270–287, 2024.
- [78] Dongyuan Song, Kexin Li, Xinzhou Ge, and Jingyi Jessica Li. Clusterde: a post-clustering differential expression (de) method robust to false-positive inflation caused by double dipping. *Research Square*, 2023.
- [79] Jiaqiang Zhu, Lulu Shang, and Xiang Zhou. Srtsim: spatial pattern preserving simulations for spatially resolved transcriptomics. *Genome biology*, 24(1):39, 2023.
- [80] Dongyuan Song, Qingyang Wang, Guanao Yan, Tianyang Liu, Tianyi Sun, and Jingyi Jessica Li. scdesign3 generates realistic in silico data for multimodal single-cell and spatial omics. *Nature Biotechnology*, 42(2):247–252, 2024.